KfK 4449
September 1988

Formation of Titanium Nitride Layers on Titanium Metal: Results of XPS and AES Investigations

H. Moers, G. Pfennig, H. Klewe-Nebenius,
R.-D. Penzhorn, M. Sirch, E. Willin
Institut für Radiochemie

Kernforschungszentrum Karlsruhe

KERNFORSCHUNGSZENTRUM KARLSRUHE

Institut für Radiochemie

KfK 4449

Formation of Titanium Nitride Layers on Titanium Metal: Results of XPS and AES Investigations

H. Moers*, G. Pfennig, H. Klewe-Nebenius,
R.-D. Penzhorn, M. Sirch, E. Willin

* Present address: Hoechst AG
Werk Kalle
Postfach 35 40
D-6200 Wiesbaden 1

KERNFORSCHUNGSZENTRUM KARLSRUHE GMBH, KARLSRUHE

Kernforschungszentrum Karlsruhe GmbH
Postfach 3640, 7500 Karlsruhe 1

ISSN 0303-4003

Formation of Titanium Nitride Layers on Titanium Metal: Results of XPS and AES Investigations

Abstract

The reaction of titanium metal with gaseous nitrogen and ammonia at temperatures of 890 °C leads to the formation of nitridic overlayers on the metallic substrate. The thicknesses of the overlayers increase with increasing reaction time. Under comparable conditions ammonia reacts much slower than nitrogen.

XPS and AES depth profile analyses show continuous changes of the in-depth compositions of the overlayers. This can be interpreted in terms of a very irregular thickness of the overlayers, an assumption which is substantiated by local AES analyses and by the observation of a pronounced crystalline structure of the substrate after annealing pretreatment, which can give rise to locally different reaction rates. The depth profile is also influenced by the broad ranges of stability of the titanium nitride phases formed during the reaction.

The quantitative analysis of the titanium/nitrogen overlayers by AES is difficult because of the overlap of titanium and nitrogen Auger peaks. In quantitative XPS analysis problems arise due to difficulties in defining Ti 2p peak areas. This work presents practical procedures for the quantitative evaluation by XPS and AES of nitridic overlayers with sufficient accuracy.

Bildung von Titannitrid-Schichten auf Titanmetall: Ergebnisse von XPS- und AES-Untersuchungen

Zusammenfassung

Die Reaktion von Titanmetall mit gasförmigem Stickstoff und gasförmigem Ammoniak bei 890 °C führt zur Bildung von nitridischen Deckschichten auf dem metallischen Substrat. Die Dicken der Deckschichten nehmen mit steigender Reaktionszeit zu. Unter vergleichbaren Bedingungen ist die Reaktion mit Ammoniak bedeutend langsamer als die mit Stickstoff.

XPS und AES Tiefenprofil-Messungen zeigen kontinuierliche Veränderungen der Tiefenverteilungen der Elemente Titan und Stickstoff innerhalb der Deckschichten. Dies beruht vermutlich auf der sehr unregelmäßigen Dicke jeder einzelnen Deckschicht. Diese Vermutung wird unterstützt durch die Ergebnisse von AES-Punktanalysen und durch die Beobachtung einer ausgeprägten kristallinen Struktur des Substrats nach der thermischen Vorbehandlung, was zu lokal unterschiedlichen Reaktionsraten Anlaß geben kann.

Die quantitative Analyse von Proben, die neben Titan Stickstoff enthalten, wird in der AES durch die Überlagerung von Titan- und Stickstoff-Augerübergängen erschwert. In der XPS treten Schwierigkeiten bei der Festlegung der Ti 2p-Peakflächen auf. In dieser Veröffentlichung werden Verfahren vorgestellt, die die quantitative Auswertung sowohl von XPS- als auch von AES-Spektren erlauben und Daten hinreichender Genauigkeit liefern.

I. Introduction

Titanium metal has several properties of interest for its application in the fuel cycle of a fusion reactor. For instance, its capability of reversibly forming titanium hydrides (1-3) can be employed for the storage and handling of gaseous tritium. In addition, its excellent gettering characteristics may be used to remove impurities from the burned fuel of a fusion reactor (4). In both applications detailed kinetic information on the reaction of metallic titanium with gaseous impurities such as N_2, NH_3, CO, CO_2, CH_4 etc., which play a role during the fusion fuel cycle, is of major importance. While for gettering purposes the occurrence of irreversible reactions with these gases is desired to achieve an optimal cleaning effect, in the case of tritium storage the formation of surface titanium compounds (nitrides, oxides, carbides) is likely to influence significantly the rate and capacity of tritium uptake. Another area of interest involves coating of titanium by nitridation, which is known to produce a corrosion resistant surface.

The present investigation of the reaction of nitrogen compounds with titanium is part of a program, which aims at the determination of the kinetic parameters and the identification of the reaction products of potential candidate metal and alloy getters with impurity gases of the fusion fuel cycle. The examination of titanium nitrides and nitrided titanium surfaces by modern instrumental analysis such as X-ray photoelectron spectrometry (XPS) and Auger electron spectrometry (AES) has received considerable attention in the recent literature (5-15). Other fields of application of these two and of other surface sensitive techniques in fusion technology can be found in refs. (16-18). This work concentrates on XPS and AES investigations of the reaction of titanium metal with nitrogen and ammonia and describes the composition and depth distribution of the reaction products. Both techniques are extremely surface sensitive for the detection of surface species and thus very well suited to characterize the interactions at the interface between a solid and a gas phase. Particularly together with X-ray diffraction XPS and AES provide quantitative chemical information on the surface products. In combination with ion bombardment induced sputtering they give access to several micrometer thickness of the surface layer of a solid.

II. Experimental

The titanium samples investigated in this work were either small cuttings (size $\approx$ 2 x 6 mm^2, sample 1) or squares (size 10 x 10 mm^2) of 0.25 mm thick foils, which were supplied by Vakuumschmelze Hanau (samples 2 and 3) or by Goodfellow Metals, Cambridge (samples 4-8), respectively. The purity of the foils from the latter manufacturer was stated to be 99.6 % Ti.

Prior to exposure to nitrogen or ammonia the Ti samples were annealed in a quartz vessel under vacuum at 890 °C for several hours. In experiments 1-2 the metallic samples were first allowed to cool down to room temperature. Then the reacting gas was introduced into the quartz vessel and the sample heated up to the reaction temperature under isochoric conditions (V = 0.668 l). With progressing reaction a small pressure drop due to nitrogen consumption was observed. An analogous procedure was employed in experiment 3 except that in this case, due to the formation of H_2 and N_2 by cracking of NH_3, the gases were circulated over the metallic sample with the help of a Metal Bellows pump. In runs 4-8 the reacting gas was admitted to the hot sample immediately after completion of the annealing treatment. The kinetic study itself was carried out under isobaric conditions employing a Balzers RME-010 pressure reducing valve, which permitted a regulation of the pressure to $\pm$ 5 mbar. The gas consumption was followed volumetrically employing calibrated vessels and an MKS-Baratron 170 M capacitance manometer.

At the end of each experiment the gas was pumped off and the quartz reaction vessel cooled down to room temperature. The samples were then stored under a dry inert gas inside a glove box until needed for surface analysis. Further details concerning the annealing and reaction conditions employed during experiments 1-8 are given in Table 1.

For XPS and AES measurements the specimens were mechanically mounted on appropriate specimen stubs under laboratory atmosphere and then introduced into the spectrometer. Due to the lack of an adequate sample introduction system which operates under an inert gas atmosphere, the specimens were briefly exposed to the atmosphere during this step. As a consequence the XPS spectra of the specimens showed partial oxidation of the outermost atomic layers.

The XPS and AES measurements were performed in a Vacuum Generators (VG) ESCALAB 5 electron spectrometer already described elsewhere (19). The system is equipped with a hemispherical sector field analyzer. Most measurements were

carried out at a base pressure of 10^{-9} mbar. Details of the instrumental parameters and measurement conditions employed for the recording of XPS and AES spectra as well as of depth profiles are summarized in Table 2 and Table 3. Data acquisition, storage, handling, and evaluation was carried out with a PDP 11/03 computer (Digital Equipment Corporation) employing software supplied by the manufacturer of the electron spectrometer. This software package includes the possibility of removing X-ray satellites and the background of inelastically scattered electrons. The latter is performed according to a mathematical treatment given by Shirley (21).

III. Results and Discussion

1. Microscopic examination

All samples were routinely inspected with a light microscope for possible effects of the various treatments on the appearance of the sample surfaces. This examination revealed that already during the annealing procedure structural transformations of the metal took place. For instance, Figs. 1 and 2 show microscopic photographs of the original titanium foil (representative of specimens 2 and 3) as received from the manufacturer and before annealing. Besides some black dots, which represent impurities on top of the surface, the appearance of the surface is governed by traces resulting from the mechanical treatment of the material during manufacture (probably rolling). After annealing for about 4 h the surface structure has changed markedly as can be seen in Figs. 3 and 4. Even though the working traces are still visible the surface appearance is now governed by the crystalline structure of the metal foil. This indicates that the foil itself and the heavily disturbed surface layer of the metal foil, resulting from the mechanical treatment during manufacture, have recrystallized during annealing. The X-ray diffraction spectrum of the annealed titanium foil (4 h at 890 °C) shows no significant difference from that obtained with the untreated foil. Only heating up to higher temperatures (> 920 °C) causes permanent changes of the crystallographic structure.

Exposure of the Ti foil to nitrogen at 890 °C does not significantly alter the appearance of the surface. This is apparent from a comparison between photographs of specimen 2 before (Figs. 3 and 4) and after reaction with nitrogen (Figs. 5 and 6).

The appearance of the surface is not affected by ion bombardment applied during the measurements of the AES depth profiles. Figs. 7, 8 and 9 show photographs of that part of the surface, which has been hit by the ion beam. The approximately

rectangular slightly brighter area in the center of Fig. 7 corresponds to the ion bombarded part of the surface. Figs. 8 and 9 show sections of this area at higher magnifications.

A comparison of the light microscopic photographs with those obtained with a scanning electron microscope (SEM) employing a rastered electron beam for the excitation of secondary electrons gives additional information. The resolution achieved with the SEM was of the order of one micrometer. Figs. 10 and 11 show SEM micrographs of sample Nr. 2. The shown area is close to the sputter crater. When compared to Figs. 5 and 6 it is seen that whereas the light microscopic photographs predominantly show the typical features of the crystalline structure, the SEM micrographs are dominated by the working traces from the manufacture of the metal foil, the crystalline structure being only barely recognizable (see Fig. 11). Due to their low kinetic energy secondary electrons can only be emitted from a surface layer of a few nanometers thickness. Furthermore, the contrast in SEM pictures is governed by gross differences in chemical composition and/or the topography of the sample surface. Therefore, the absence of significant differences between different crystallites in the SEM pictures indicates a fairly homogeneous composition of the upper sample surface layer, which is not apparent from the light microscopic examination.

Within the ion bombarded area, on the contrary, the SEM micrographs show a surface with a distinct crystalline structure. The SEM micrograph in Fig. 12 shows approximately the same section of the foil as the light microscopic photograph in Fig. 7. The SEM micrograph in Fig. 13, which was obtained with a higher magnification than that in Fig. 12, depicts an area close to the center of the sputter crater. Approximately the same zone is also shown in the light microscopic photograph of Fig. 9. The shadowing effects along the grain boundaries indicate significant topographical height differences.* These height differences appear only after extended ion bombardment of the sample suggesting that the sputtering rates depend upon crystallite orientation.

2. AES: Depth profiles

The major Auger transitions of titanium are observed at kinetic electron energies of about 385 eV ($L_3M_{23}M_{23}$) and 420 eV ($L_3M_{23}V$), the most prominent one of nitrogen occurs at about 385 eV ($KL_{23}L_{23}$). Therefore an almost complete overlap

---

* The light microscopic photographs of the titanium foils obtained from other manufacturers (samples 4-8) showed essentially the same features as the ones already described. They are, therefore, not discussed separately in this section.

of the Ti ($L_3M_{23}M_{23}$) and N($KL_{23}L_{23}$) transitions is expected in the Auger spectra of samples containing both titanium and nitrogen. This is illustrated in Fig. 14, in which the AES spectra of titanium and titanium mononitride are compared. The latter spectrum shows the surface composition of a pellet, which was pressed from commercial TiN powder and which was sputtered in the electron spectrometer until a constant surface composition was achieved.

The considerable amount of oxygen present in the sample results from partial oxidation of the surfaces of the individual grains when the powder gets in contact with air during manufacture of the pellets. Sputtering can only remove oxygen from the outer surface of the pellet but not that incorporated into the pellet during compactation of the powder.

One approach to separate the contributions of titanium and nitrogen to the complex peak at 385 eV has been described by Dawson and Stazyk (9). The authors determined the intensity ratio of the two major Auger transitions of titanium metal with their instrumental parameters and assumed that any deviation from this ratio occuring after nitridation of the sample surface is due to the overlapping of the N($KL_{23}L_{23}$) / Ti ($L_3M_{23}M_{23}$) peaks. The titanium contribution to the complex peak at 385 eV is calculated from the Ti ($L_3M_{23}V$) / Ti ($L_3M_{23}M_{23}$) metal ratio and the height of the peak at 420 eV. The difference between the total height of the peak at 385 eV and the height attributed to the Ti contribution is assigned to the intensity of the N($KL_{23}L_{23}$) Auger peak. The various phases formed during the gas/metal reaction were identified by X-ray diffraction. Uncertain with this method is the dependency of the intensity ratio (ratio of excitation probabilities) of the titanium peaks on the chemical environment of the sample. For example it is known from experiments with titanium oxides that the Auger peak Ti ($L_3M_{23}M_{23}$) /Ti ($L_3M_{23}V$) intensity ratio varies significantly with the state of oxidation of titanium (22,23).

In this work another evaluation procedure based on the use of two appropriate reference materials is discussed. In addition to the assumption that the ratios of the excitation probabilities remain constant, the approach requires a knowledge of the relation of the absolute intensities of the Auger peaks of the two reference materials.

In the case of TiN_x the intensity ratios of the two Auger transitions of titanium and of a titanium nitride of known composition can be employed. The stoichiometry of the unknown sample can be derived from the experimentally observed intensity ratios of these two reference materials as well as the one from the titanium nitride

phase under investigation. Under the assumption that the intensity increase of the Auger transition at 385 eV is proportional to the nitrogen uptake of the sample a straight forward evaluation is possible, i.e. the nitrogen concentration of the sample under investigation is obtained from the measured intensity ratio of the peaks at 420 and 385 eV. Any sample with a nitrogen concentration lower than that of the mononitride will exhibit an Auger spectrum with an intensity ratio value lying between that of the mononitride and that of the pure metal. As apparent from Fig. 14 the intensity ratios of the metal and of the mononitride differ significantly. Therefore, a sensitive determination of the composition of the nitrided samples is possible.

Starting from the assumption that the spectrum of an unknown compound TiN_x results from the overlap of the spectra of Ti metal and TiN, the following expression for the peak intensity ratio S (peak at 420 eV to peak at 385 eV) of the sample under investigation can be derived

$$S = \frac{(\frac{1}{x} - 1) + C}{(\frac{1}{x} - 1)\frac{1}{T} + \frac{C}{N}} \qquad (1)$$

In this expression T and N are the intensity ratios (420 eV/385 eV) of the titanium metal (T = 1.24) and of the mononitride (N = 0.52), respectively. C is a constant which accounts for the different absolute intensities of the Auger transitions of the reference materials. C, which was simply equated to the ratio of the atomic concentrations of titanium in the mononitride and in the metal, was calculated to be 0.9. Implicit in this calculation is the assumption that the Auger transition intensity is proportional to the atomic concentration of the species under investigation. Equation (1) is based on purely stoichiometric considerations:

$$TiN_x \rightarrow Ti_{1/x}N = (\frac{1}{x} - 1)\,Ti + TiN$$

By simple rearrangement of eq. (1) an expression can be obtained, which permits the calculation of the average composition of a sample from a knowledge of the intensity ratios S, T, and N as obtained from the corresponding Auger spectra:

$$x = \frac{S/T - 1}{S/T + C\,(1 - S/N) - 1} \qquad (2)$$

Fig. 15 illustrates the evaluation of the average stoichiometry of the analyzed volume as a function of the 420 eV peak / 385 eV peak ratio S employing eq. (2). Several possible sources of error need to be kept in mind when using eq. (2) or Fig. 15:

- uncertainty in the intensity ratios of the reference materials, in particular TiN (oxygen contribution)
- uncertainty in the absolute intensities of the Auger peaks of the reference materials (no experimental data available yet, the effect of changing C is illustrated in Fig. 15)
- uncertainty concerning chemical effects influencing the experimentally determined intensity ratios
- neglection of the fine structure of the Auger peaks for the evaluation of intensity ratios (see Fig. 14 and the peak heights defined therein).

Figs. 16 - 23 show the depth profiles recorded for each sample along with representative Auger spectra obtained at selected depths. The peak heights have been used as defined in Fig. 14 without consideration of possible contributions from the fine structure of the spectra. A conversion of the peak heights into TiN_x compositions can be done by using Fig. 15 or eq. (2). The depth scale has been estimated from the actual ion current densities and the measured sputtering rates of titanium metal and titanium dioxide (see Table 3).

The Auger spectra as well as the depth profiles of the various samples show that their surfaces are partly oxidized. In addition, the surfaces show adsorbed hydrocarbons. Both surface contaminants (oxygen and carbon), which result from the contact of the samples with atmosphere, are easily removed after short sputtering. As a rule, both elements practically disappear from the AES spectra after removing a 10 - 20 nm surface layer, leaving titanium and nitrogen as the only detectable elements and suggesting the formation of one (or several) titanium nitride(s). In fact, the AES spectra recorded just after the removal of carbon and oxygen closely resemble that of TiN (see Fig. 14 b). The presence of nitrides is, in addition, substantiated by the characteristic XPS chemical shifts of nitrogen and titanium (see section 3).

The intensities of the Auger transitions at 420 eV and 385 eV kinetic energy, which correspond, on one hand, to a titanium transition alone and, on the other hand, to the overlapping of a titanium and a nitrogen transition, show in each of the examined depth profiles continuous variations over the whole depth range

investigated, indicating that the nitrogen contribution to the spectra continuously decreases with progressing depth. Several explanations can account for these observations:

- The overlayer formed during the reaction between titanium and nitrogen actually shows the observed compositional gradient over the depth range. In principle, this is possible because titanium nitride phases are stable within a very broad range of concentrations (24).
- The overlayer thickness is strongly dependent upon the location at the surface at which it was formed. Since AES spectra only yield the integral composition of a certain surface area, large thickness differences within the analyzed area can also give rise to the observed depth profiles.
- A combination of the former two explanations.

Additional distortion of the depth profiles can be caused by lateral variations in the sputtering yields and thus of the sputtering rates. However, this is considered to be a secondary effect, which will only play a role when significant variations in lateral composition occur.

No conclusive interpretation of the reaction mechanism is possible on the basis of the experimental data available. Probably, both effects discussed above contribute to some extent to the experimental observations. Because of the pronounced crystalline structure shown by the surface of the foils after annealing (cf. Chapt. III.1.), the possibility of different reaction behaviour at the various crystal faces, leading to variations in the product layer thickness and perhaps to several product nitrides, need to be considered. For instance, local AES analyses of sample No. 7 at a depth of approx. 4 μm indicate large variations in lateral composition. However, these observations do not exclude a possible contribution from in-depth gradients to the depth profiles.

While the absolute depth ranges of the examined samples showed significant variation with reaction time and type of reacting gas, no fundamental differences between the shapes of the various depth profiles could be observed. This is apparent from a comparison of samples No. 2, 3 and 5. The only difference between samples No. 2 and 5, which reacted with nitrogen, and sample No. 3, which reacted with ammonia, is that in the latter case the amount of nitride formed is smaller (see Figs. 17, 18 and 20).

The average composition of the overlayer as a function of depth can be derived using Fig. 15 or eq. (2). Table 4 summarizes the estimated compositions of the overlayer of all investigated samples at progressing depths. In addition, the position of the point of intersect on the depth scale, i.e. the depth at which the Auger transitions at 420 and 385 eV are equally intense, is included. This intersect, which corresponds to a composition of $TiN_{0.19}$, has been arbitrarily defined as the thickness of the nitridic overlayer. The intersects for samples 2, 3 and 5 were observed to occur at 880, 200 and 790 nm, respectively, indicating that under comparable conditions nitrogen penetrates deeper into the titanium metal than ammonia. Generally, an increase in reaction time is accompanied by a shift of the position of the intersect towards greater depths and, in consequence, by an increase of the thickness of the reaction product layer.

The initial part of the depth profile of sample No. 4 (and to a lesser extent of sample No. 5) differs from those of the other samples in that the intensity of the Auger peak at 385 eV passes through a maximum very close to the surface. This points to a relatively high nitrogen concentration in the surface layer of these samples. It is not clear why only these samples show such an effect. Presumably this is related to the particularly short reaction time selected for these experiments. Since all samples were first heated up to 890 °C before admitting nitrogen into the reaction vessel, they cooled down when brought in contact with the non-preheated gas. In the case of experiments of short duration this retardation in heating manifests itself rather strongly on the total reaction time. In consequence, runs like that with sample No. 4 do not reflect constant temperature conditions for the reaction and diffusion process over the stated period of time (in experiments of longer duration the initial departure from steady state conditions can be neglected). A more detailed investigation is necessary for a complete elucidation of this effect.

Depth regions of constant composition were observed only in the profiles of samples No. 7 and 8. The ranges extend approx. from 300 - 1200 nm (sample No. 7) and from 300 - 1700 nm (sample No. 8), respectively (cf. Table 4). The extension of the profile region with constant composition is, however, small compared to the total depth of the overlayer where nitrogen can be detected. Sample No. 7 has also been investigated by XPS. The depth profile resulting from these measurements is displayed in Chapt. III.3 (cf. Fig. 29) and compares well with the results from the AES depth profile.

3. Surface analysis and depth profiles by XPS

In addition to the AES depth profile measurements several samples were investigated by XPS with the aim of characterizing the surface and speciating the overlayer constituents. The method also permits a determination of depth distributions. Due to the difficulties encountered during the quantitative evaluation of the AES spectra (see Chapt. III.2) useful complementary information was expected from this surface analysis technique.

Fig. 24 shows an XPS spectrum of sample No. 7. The surface shows contributions of titanium, nitrogen, oxygen and carbon. While the overwhelming fraction of the carbon can be attributed to a contamination of the sample surface by hydrocarbon adsorption during contact of the specimens with air, a small additional peak at the binding energy position corresponding to titanium carbide can also be observed. It is very likely that this compound has been formed during the thermal treatment of the sample (annealing and/or reaction step). Possible reaction partners are carbon containing impurities (hydrocarbons or carbon oxides) in the gas phase or adsorbed at the metallic substrate prior to the thermal treatment.

The titanium 2p photopeaks clearly show the presence of two titanium species, which we attribute to titanium nitride (not necessarily stoichiometric) and to some titanium oxinitride of unknown composition. On the basis of the observed binding energy shifts the presence of pure titanium dioxide can be excluded.

Table 5 summarizes the binding energies determined experimentally for the surface compositions of several titanium specimens as well as of the standard materials employed in this work. The N 1s photopeak appears at a binding energy of 396.9 eV. This binding energy, which is indicative of a nitride, compares well with the values from our own standard and with those reported in the literature (a compilation of literature values is given in Table 6).

The XPS measurements were also employed for the determination of depth profiles. For this purpose a quantitative evaluation of the (relative) concentrations of titanium in the titanium containing materials is required. The major difficulty is to find a reliable way to determine the peak area of the titanium 2p photopeaks. The problem is caused by the presence of intense loss features in the Ti 2p spectrum of titanium and titanium compounds, which originate from the excitation of surface and volume plasmons and/or from shake-up processes (15). Shake-up processes are the result of the excitation of valence electrons into unfilled levels.

They occur simultaneously with photoemission processes of the excited atom (28). The shake-up satellites represent photoelectrons which have lost energy during their emission by a secondary excitation of the atom. Therefore the intensity of the satellites should be added to the total photoemission intensity. Plasmon excitations, on the contrary, are associated with loss processes, taking place when electrons pass through a solid (29). They are comparable to inelastic energy losses of electrons (the latter giving rise to the background). Plasmon excitations are not associated with the primary excitation processes within the atom and should, for this reason, not be considered as part of the photoelectron emission intensity (30).

The overlap of loss structures from plasmon and shake-up excitations in the XPS spectra of titanium nitride, titanium metal (15) and presumably titanium oxinitrides, the latter being of relevance only for surface-near atomic layers, makes it impossible to define accurately the part of the total photopeak structure necessary for the determination of the peak area (or photoemission intensity, respectively). In view of this, a practical but somewhat arbitrary procedure for the determination of the peak area was developed.

A typical evaluation of a depth profile is illustrated utilizing the Ti 2p XPS spectra of sample No. 3 measured at various depths (see Fig. 25). As apparent from the spectra the surface oxidation product has already disappeared after a very short sputtering period e.g. after removing a few nanometers of surface material. At 50 nm the spectrum closely resembles that of titanium metal except for the fact that the peak positions are slightly shifted and that the intensity of the N 1s photopeak indicates the presence of a considerable amount of titanium nitride.

The peak area determination is carried out in several consecutive steps as illustrated in Figs. 26 and 27 for the case of two Ti 2p spectra from Fig. 25 (depth 0 and 0.4 nm, respectively). In a first step the background attributed to the inelastic scattering of the electrons is subtracted. This contribution is calculated from equations as proposed by Shirley (21). Figs. 26 a and 27 a show the raw data as well as the calculated background. In Fig. 26 a the intensities of the raw spectrum and of the background spectrum coincide at a binding energy which corresponds to the intensity minimum at the high binding energy side of the photopeak multiplet. This is where one would approximately expect the upper limit of the energy range of the multiplet. Fig. 26 b shows the spectrum after subtraction of the background and, in addition, after subtraction of the X-ray satellites (spacings and relative intensities taken from Ref. (31)). The hatched part of the resulting spectrum gives the peak area ascribed to the intensity of the phototransition. The broad peak on

the right part of Fig. 26 b is assigned to plasmon losses not contributing to the photoemission intensity.

In the case of the XPS spectrum shown in Fig. 27 the situation is more complicated. Fig. 27 b shows the multiplet resulting after subtraction of the background and the satellite. For the determination of the peak area there is clearly no minimum at the right binding energy side of the multiplet which might serve as a limit to distinguish between the photopeak multiplet and the plasmon structure contribution. Consequently, it was assumed that the spectrum results from an overlap of both contributions as represented by the dashed lines in Fig. 27 b. The intersect was assumed to occur at the same binding energy position as the minimum in Fig. 26 b. Postulating a symmetrical overlap, a peak area as indicated by the hatched area in Fig. 27 c can be derived.

With the procedure described above reproducible and consistent peak areas from Ti 2p XPS spectra can be determined. The evaluation method neglects any shake-up satellites which might occur in the energy range of the plasmon structure and which actually are present for instance in the XPS spectra of titanium dioxide in the relevant energy range (15,20,25,32). Also neglected is that fraction of the plasmon structure which might appear below the photopeak multiplet. It is expected that both errors cancel out to some extent. In absence of a more accurate evaluation method of the peak areas from the Ti 2p XPS spectra the chosen procedure provides reasonably good data for the determination of the composition because the comparison of consistently evaluated data is possible with better precision.

The depth profiles of sample No. 3 and No. 7, which were evaluated according to the procedure described above, have been plotted in Figs. 28 and 29, respectively. Fig. 28 shows the intensities of the Ti 2p, N 1s, O 1s, and C 1s phototransitions (left ordinate) and the Ti/N atomic ratios (right ordinate, calculated from the absolute intensities after correction for the photoionization cross sections as given by Scofield (33)) as a function of depth. While the dash-pointed curve has been determined from the total intensity of the Ti 2p transition, the pointed curve includes a correction for the fraction of titanium bound to oxygen. Because oxygen is rapidly removed, the two curves diverge only over the first ten nanometers in depth. Fig. 29 gives the Ti/N atomic ratio over a depth range of approx. 2 µm of sample No. 7. In this case the contribution of oxygen can be neglected except for the first 30 nm.

The results plotted in Figs. 28 and 29 point to an approximate stoichiometry of Ti_2N. Only very close to the surface the stoichiometric coefficient approaches unity suggesting a composition of the surface nitride close to TiN. None of the samples shows constant composition over the analyzed depth range. In some samples, for instance sample No. 7, only a small concentration gradient at depths between 200 and 1500 nm was observed. This range of approximately constant composition was also observed by an AES characterization of sample No. 7 (cf. Table 4 and discussion in Chapt. III.2).

During the measurements of the depth profiles a continuous binding energy shift of the Ti $2p_{3/2}$ photopeak towards the value of titanium metal became apparent, which correlates with the composition of the analyzed volume (see Fig. 30). The curve in Fig. 30, which is based on the depth profiles shown in Figs. 28 and 29, reflects a dependence of the binding energy upon composition. Also included in Fig. 30 are three data points from the titanium mononitride reference sample (before and after sputtering) as well as data found in the literature. Particularly, the latter show a considerable scatter in binding energies. As opposed to this the values obtained in this work show a smooth variation with composition.

In principle, the observed binding energy shift can be ascribed to changes in the chemical environment of a homogeneously composed phase or to changes in the average composition of a mixture of phases (titanium metal and titanium nitride). In the latter case the position of the binding energy scale of the Ti 2p peak maxima would be the result of the overlap of the Ti 2p spectra of different species and the value of the binding energy would depend on the relative intensities of the overlapping spectra. The results from the AES measurements (cf. Chapt. III.2) favour the second explanation, i.e. differently composed phases. In this case a dependence of the binding energy shifts on the composition of the titanium nitride is expected, particularly in the low nitrogen concentration ranges. Unfortunately, the large scatter of the literature values (cf. Fig. 30 and Tab. 6) does not allow an unequivocal conclusion. In addition, binding energies for nitrogen concentrations below 40 at.% are not available. Possibly, the dependence displayed in Fig. 30 is the result of both effects described above.

4. Comparison of the surface analysis results with kinetic measurements

Tab. 7 summarizes the nitridic overlayer compositions, which have been derived from AES and XPS measurements of the various samples; the fourth column shows phases detected by X-ray diffraction. As evident from the results, the XPS and the AES measurements are in reasonably good agreement. Especially in the depth range of approximately constant composition (see for example the range between 300 and

1200 nm of sample No. 7) both techniques point to a composition of about $TiN_{0.5}$. A composition approaching that of TiN appears to occur only at the surface of each sample but with increasing depths the nitrogen concentration shows a continuous decrease (cf. Tab. 4).

To understand the apparent compositional discrepancies observed when nitrided titanium specimens are characterized by XPS, AES and X-ray diffraction, it is necessary to take into account that, whereas XPS and AES provide only the average composition of the analysed volume, X-ray diffraction is capable of identifying single phases (see Tab. 7). Accordingly, it was observed that after a short exposure to nitrogen the reflections of the specimens can be assigned to αTi and Ti_2N and that after a prolongued exposure additional reflections characteristic to TiN appear. This is certainly not in disagreement with the depth profiles determined by AES. As a whole, the results point to a layered structure of TiN over Ti_2N and αTi.

The depth profiles show that the thickness of the overlayer is not too well defined. The overlayer thickness was assumed to be given by the position on the depth scale of the intersect at equal intensity of the two predominant Auger lines. The positions of the intersects are given by the fifth column in Tab. 7 and are displayed as a function of reaction time in Fig. 31.

The data in Tab. 7 suggest that under comparable conditions the rate of the reaction of ammonia is much slower than that of nitrogen. This result, which is in disagreement with the observations of other authors (34), may be explained by the occurrence of significant cracking of ammonia, i.e.

$$2\,NH_3 \rightarrow N_2 + 3\,H_2$$

on the surface of the titanium sheets. Such a reaction has been observed to occur at 625 °C with a rate constant of $k = (3.1 \pm 1.9) \cdot 10^{13}$ molecules/cm² · sec (35). Since the gas / metal reaction was followed under static conditions, it is expected that the products of the reaction, i.e. H_2 and N_2, will cumulate in the vicinity of the metal surface and retard the reaction.

The nitrogen uptake observed when titanium foils react with nitrogen at 890 °C was measured volumetrically and is shown graphically in Fig. 32. In general, an induction period of a few minutes was observed, which is due to a decrease in temperature of the metallic sample when brought in contact with the non-preheated gas. The reaction rate can be described by a parabolic law of the type

$$w^2 = K \cdot t$$

where

w = weight gain/area
K = temperature dependent proportionality constant
t = time

and the constant K has a value of (10.1 ± 0.3) $\mu g^2/cm^4 \cdot sec$ at 890 °C. The curve showing the time dependency of the depth profiles as determined by AES is similar to the one obtained from the weight gain experiments (see Table 8 and Figs. 31 and 32). A comparison between the overlayer thickness as estimated from AES measurements and that calculated with the data in Table 8 and crystallographic considerations, assuming a layer of either the composition TiN or Ti_2N is given in Table 7. Considering that the overlayer thickness determined by AES is based on estimated sputtering rates and was arbitrarily assumed to end at the depth at which the main Auger transitions are of equal height and that the thickness estimated from weight gain runs was obtained under the assumption of a homogeneous single phase (TiN or Ti_2N) overlayer, the agreement can be considered satisfactory.

One result of the XPS measurements was the observation of a direct dependence of the binding energy shift of the Ti 2p photopeaks upon the nitrogen concentration of the nitrided surface. It is at present not clear whether this effect arises from the compositional change of a homogeneous phase or is caused by the overlapping of Ti 2p spectra of several species of varying concentrations. More work is needed to shed light on this question.

Acknowledgements

We are grateful to U. Berndt for taking the X-ray diffraction spectra.

Table 1: Annealing and reaction conditions employed in experiments on the interaction of titanium metal with nitrogen and ammonia

	annealing step				reaction step			
experiment/ sample No.	duration (h)	pressure (mbar)	temperature (°C)	reactant	starting pressure (mbar)	heat-up phase (min)	holding phase (h)	temperature holding phase (°C)
1[a]	-	-	890	N_2	130	-	24	890
2	4	$3{,}7 \cdot 10^{-5}$	890	N_2	135.5	100	0.50	890
3	4	$3 \cdot 10^{-5}$	890	NH_3	135	40	0.62	890
4	4	$1 \cdot 10^{-5}$	890	N_2	135 ± 2[b]	-	0.25	890
5	4	$1 \cdot 10^{-5}$	890	N_2	135 ± 2[b]	-	0.50	890
6	4	$1 \cdot 10^{-5}$	890	N_2	135 ± 2[b]	-	2.00	890
7	4	$1 \cdot 10^{-5}$	890	N_2	135 ± 1[b]	-	6.17	890
8	4	$1 \cdot 10^{-5}$	890	N_2	135 ± 1[b]	-	7.00	890

a) Sample No. 1 represents a test run. Some parameters are not known with certainty and are, therefore, not given.

b) Pressure held constant during the experiment; nitrogen was admitted after the reaction temperature had been reached.

Table 2: Instrumental parameters and experimental conditions employed for the XPS measurements

Excitation:	Al K , not monochromatized
Excitation power:	10 kV · 10 mA
Analyzed surface area:	≈ 50 mm^2
Analyzer mode:	constant analyzer pass energy (CAE)
CAE-settings:	50 eV (overview spectra)
	20 eV (element spectra)
Resolution:	1.3 eV FWHM[a] for the Au 4f photopeak at CAE = 20 eV
Energy reference:	Au $4f_{7/2}$ = 84.0 eV binding energy
Depth profiling:	
Ion gun type:	penning ion source (Leybold-Heraeus IQP 10/63); operated with argon.
Primary ion energy:	≈ 5 keV
Sputtered area of constant ion current density:	≈ 80 mm^2
Ion current densities:	≈ 150 - 200 nA · mm^{-2} (valid for area of constant ion current density)
Sputtering rate:	1 nm · min^{-1} at ion current density of 100 nA · mm^{-2} [b]

a) FWHM: full width at half maximum

b) Estimated from sputtering rates of titanium metal and titanium dioxide, taken from Ref. (20).

Table 3: Instrumental parameters and experimental conditions employed for the AES measurements

Excitation source:	rasterable electron gun (VG LEG 100)
Excitation energy:	3 or 5 keV
Excitation current:	2.0 μA
Electron current density:	≈ 80 nA · mm^{-2}
Analyzer mode:	constant retard ratio (CRR)
CRR-setting:	10
Modulation voltage [a]:	2.0 eV
Depth profiling:	
Ion gun type:	rasterable ion gun (VG AG 61) operated with argon
Primary ion energy:	5 keV
Ion current:	200 - 600 nA
Ion current density:	200 - 600 nA · mm^{-2}
Sputtering rate:	1 nm · min^{-1} at an ion current density of 100 nA · mm^{-2} [b]

a) Spectra recorded directly in the derivative mode using the lock-in-amplifier technique.

b) Estimated from sputtering rates of titanium metal and titanium dioxide, taken from Ref. (20).

Table 4: Composition of the investigated samples expressed as x of TiN_x as a function of depth[a)]

sample number	position of intersect b) (nm)	depth (nm)										
		50	100	200	400	600	800	1000	1500	2000	2500	3000
1	>>3600	0.73	0.77	0.77	0.73	0.65	0.65	0.62	0.58	0.54	0.53	0.50
2	880	0.68	0.57	0.57	0.33	0.26	0.21	0.16	0.11	0.08	-	-
3	200	0.62	0.36	0.19	0.08	0.06	0.03	0.03	-	-	-	-
4	460	0.57	0.46	0.32	0.20	0.16	0.14	0.14	-	-	-	-
5	790	0.57	0.56	0.43	0.30	0.23	0.19	0.16	0.12	-	-	-
6	2170	0.58	-	0.53	0.50	0.45	0.42	0.38	0.29	0.20	0.16	0.15
7	4480	0.74	0.70	0.59	0.51	0.51	0.49	0.51	0.47	0.41	0.36	0.31
8	4780	0.82	0.60	0.57	0.52	-	-	0.52	0.51	0.46	0.39	0.32

a) Determined from the intensities of the Auger transitions displayed in the depth profiles by using Fig. 15

b) Intersect corresponds to equal intensities of the Ti ($L_3M_{23}V$) Auger transition and the sum of the Ti ($L_3M_{23}M_{23}$) and N ($KL_{23}L_{23}$) Auger transitions.

Table 5 Binding energies of the photopeaks of elements detected at the surfaces of various samples and commercial reference materials (values accurate to ± 0.2 eV)

sample	Binding energy (eV)				Ref
	Ti $2p_{3/2}$	N 1s	O 1s	C 1s	
Ti^0	454.0				25
TiO_2	459.0	-	530.3[a]	-	25
TiN pellet[b]	458.3		530.2[c]	288.4[d]	
	455.2	396.9		284.8	
Nr. 3	457.9		529.8[c]	288.1[d]	
	454.9	396.9		284.4	
Nr. 7[e]	458.4		530.0[c]	284.4	
	454.9	396.9		281.7	
Nr. 7[e]	458.0		529.8	284.0	
	455.0	396.8		281.4	

a) Not given in Ref. 25; private communication.

b) For details on sample preparation and characterization see section III.2.

c) Energy position of maximum; shoulder on high binding energy side indicates the presence of hydroxide.

d) In addition to hydrocarbons a component at the position corresponding to the binding energy of carbonate was detected.

e) Two independent measurements performed.

Table 6: XPS parameters of titanium nitrides (literature values)

compound		binding energy				calibration	
bulk comp.	assignment	Ti $2p_{3/2}$	N 1s	O 1s	Ti $2p_{3/2}$ - N 1s	line (binding energy eV)	Ref.
$TiN_{0.95}$	TiN_xO_y	458.8±0.1	-	n.g.	-	C 1s (285.0)	6[a]
	$TiN_{0.95}$	456.0±0.1	397.1±0.1		58.9		
$TiN_{0.80}$	TiN_xO_y	458.6±0.1		n.g.			
	$TiN_{0.80}$	456.1±0.1	397.3±0.1		58.8		
$TiN_{0.60}$	TiN_xO_y	458.5±0.1		n.g.			
	$TiN_{0.60}$	456.2±0.1	397.4±0.1		58.8		
$TiN_x(x \simeq 1)$	Ti(oxidized)	n.g.		n.g.		Ti $2p_{3/2}$ from	5[a]
	TiN_x ($x \simeq 1$)	455.3±0.2	n.g.		-	metal (453.8)	
$TiN_{0.9}$[b]	TiO_2	458.8		530.0		C 1s (284.6)	12[a]
	$TiN_{0.9}$	454.8[c]	n.g.		-		
TiN_1[d]	TiN_1	455.0±0.2	397.2±0.2		57.8	Au $4f_{7/2}$ (83.8)	15
						Cu $2p_{3/2}$ (932.4)	
	TiN_x ($x \simeq 1$)[e]	455.2±0.2	397.1±0.2		58.1		
$TiN_{0.99}$[f]	$TiN_{0.99}$	455.1	397.4		57.7	Ti $2p_{3/2}$ from	11
$TiN_{0.80}$	$TiN_{0.80}$	455.1	397.4		57.7	metal (453.6)	
n.g.[g]	TiO_2	457.9		530.0		C 1s (284.6)	26
	TiN_xO_y	456.7	399.9		56.8		
			398.4		58.3		
	TiN_1	454.7	396.3		58.4		
	$TiN_x(x \neq 1)$		395.4		59.3		
TiN[h]	TiN[h]	455.5	n.g.		-	Au $4f_{7/2}$ (83.8)	27
n.g.[i]	TiO_2	458.8		530.2		C 1s (285.0)	7
	TiN_x ($x > 1$)	457.3	395.8		61.5		
	TiN_1	455.5	397.2		58.3		
TiN[k]	TiN_xO_y	458.3		530.2		Au $4f_{7/2}$ (84.0)	this
	TiN_1	455.2	396.9		58.3		work
TiN[l]	TiN_xO_y	- [m]		530.9			this
	$TiN_{0.9}$[n]	454.8	396.9		57.9		work

a) Results obtained from the surface analysis of nitrides

b) Composition determined from an XPS depth profile

c) Binding energy value of N 1s remains unchanged after sputter cleaning

d) Commercial TiN powder used

e) Surface composition after N_2^+ ion bombardment of titanium metal

f) Sample surfaces abraded with a diamond file prior to measurements

g) Sample prepared by reactive sputter ion plating; speciations are the result of surface analysis and depth profiling by XPS

h) No details about sample composition given

i) Surface of titanium metal has been nitrided

k) TiN powder; details on preparation and characterization of the sample are given in Chapt. III.2

l) TiN powder (see k) after sputtering until equilibrium composition was reached

m) No separate oxinitride peak of Ti $2p_{3/2}$ observable

n) For the evaluation of the stoichiometry see discussion

n.g. = not given

Table 7: Composition and approximate thickness of the TiN_x overlayer formed during the reaction of titanium metal with nitrogen or ammonia

sample No.	overlayer composition AES[a]	XPS[b]	X-ray[c]	overlayer thickness (nm) AES[d]	weight gain[e]
1	$<TiN_{0.7}$	-	-	>>3600	-
2	$<TiN_{0.7}$	-	Ti_2N, αTi	880	-
3	$<TiN_{0.6}$	$TiN_{0.5}$	-	200	-
4	$<TiN_{0.6}$	-	Ti_2N, αTi	460	560 - 1150
5	$<TiN_{0.6}$	-	Ti_2N, αTi	790	220 - 460
6	$<TiN_{0.6}$	-	Ti_2N, αTi	2170	1720 - 3570
7	$<TiN_{0.7}$[f]	$TiN_{0.5}$	TiN, Ti_2N, α Ti	4480	3700 - 7660
8	$<TiN_{0.8}$[f]	-	TiN, Ti_2N, αTi	4780	-

a) Compositions given correspond to upper nitrogen concentration as measured at a depth of 50 nm. For further details on the decrease of nitrogen concentration with progressing depth see Figs. 16 - 23 and Table 4.

b) Approximate composition over the depth range investigated by XPS (see Figs. 28 and 29).

c) Species as identified by X-ray diffraction.

d) Values correspond to the depth at which the Auger transitions Ti ($L_3M_{23}V$) and Ti ($L_3M_{23}M_{23}$) + N ($KL_{23}L_{23}$) are of equal intensities (intersect of the AES depth profiles). Values were taken from Table 4 and represent a composition of $TiN_{0.19}$.

e) Overlayer thickness calculated from the weight gain of the sample assuming a stoichiometry of the reaction product between TiN and Ti_2N.

f) Constant composition corresponding to $TiN_{0.5}$ observed approx. from 300 to 1200 nm (sample No. 7) and from 300 to 1700 nm (sample No. 8), respectively.

Table 8: Reaction of nitrogen with titanium at 890 °C
Ti: 10 x 10 mm plates pretreated at 890 °C for 4 h under a vacuum of 10^{-5} mbar

Reaction time (min)	N_2 pressure (mbar)	N_2 consumption (mbar·l)	Ti weight (g)	N_2 uptake (g N_2/g Ti)
15	135 ± 2	0.52	0.492	$1.22 \cdot 10^{-3}$
30	135 ± 2	0.21	0.491	$4.91 \cdot 10^{-4}$
120	135 ± 2	1.62	0.490	$3.80 \cdot 10^{-3}$
370	135 ± 1	3.46	0.480	$8.33 \cdot 10^{-3}$

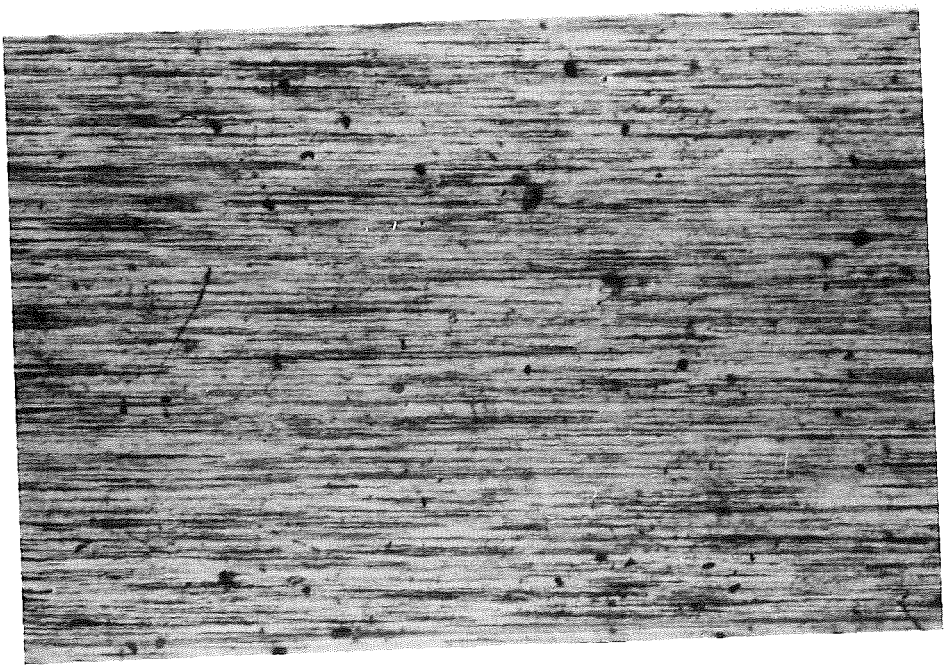

Fig. 1 Light microscopic photographs of a titanium metal foil before annealing (magnification x 50); the sample is representative of experiments 2 and 3.

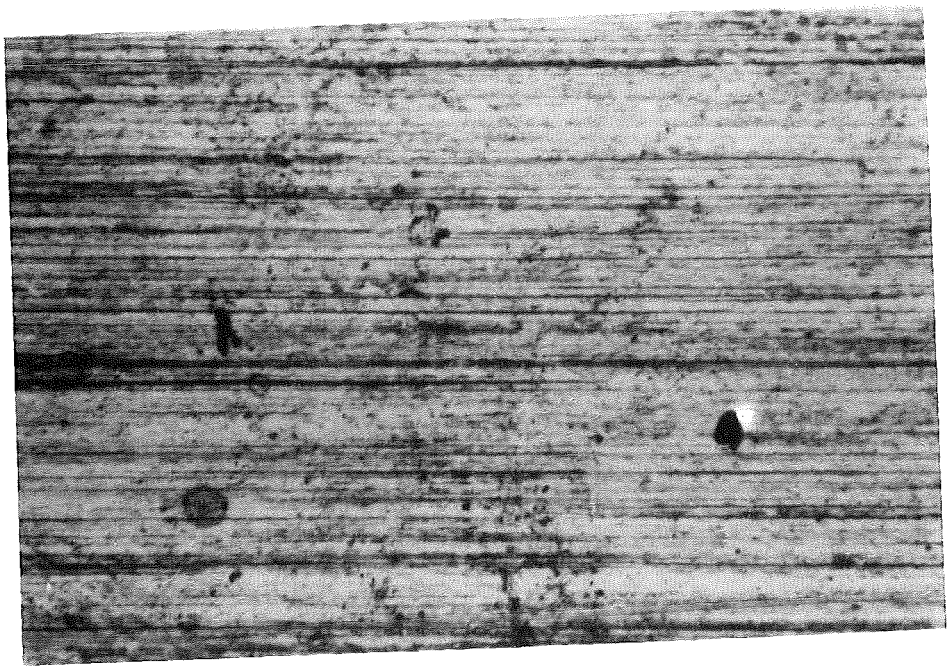

Fig. 2 Light microscopic photograph of a titanium metal foil before annealing (magnification x 200); the sample is representative of experiments 2 and 3.

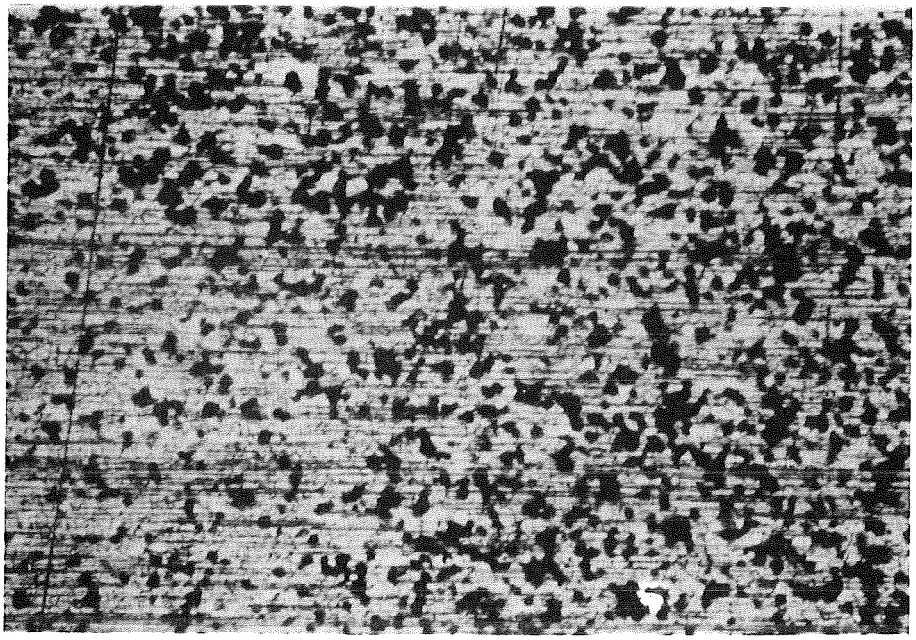

Fig. 3 Light microscopic photograph of a titanium metal foil after annealing for 4 h at 890 °C and $3 \cdot 10^{-5}$ mbar; magnification x 50.

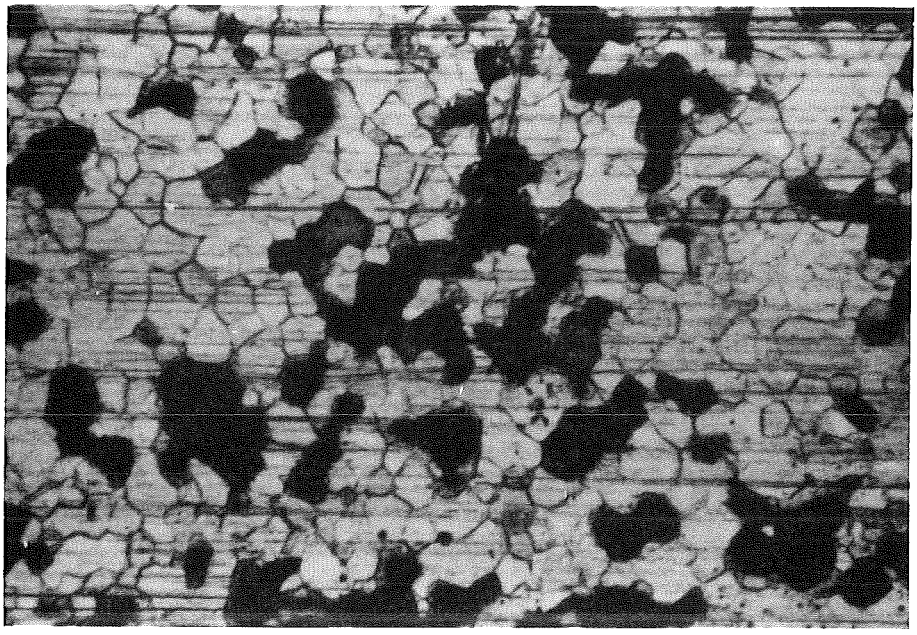

Fig. 4 Light microscopic photograph of a titanium metal foil after annealing for 4 h at 870 °C and $3 \cdot 10^{-5}$ mbar; magnification x 200.

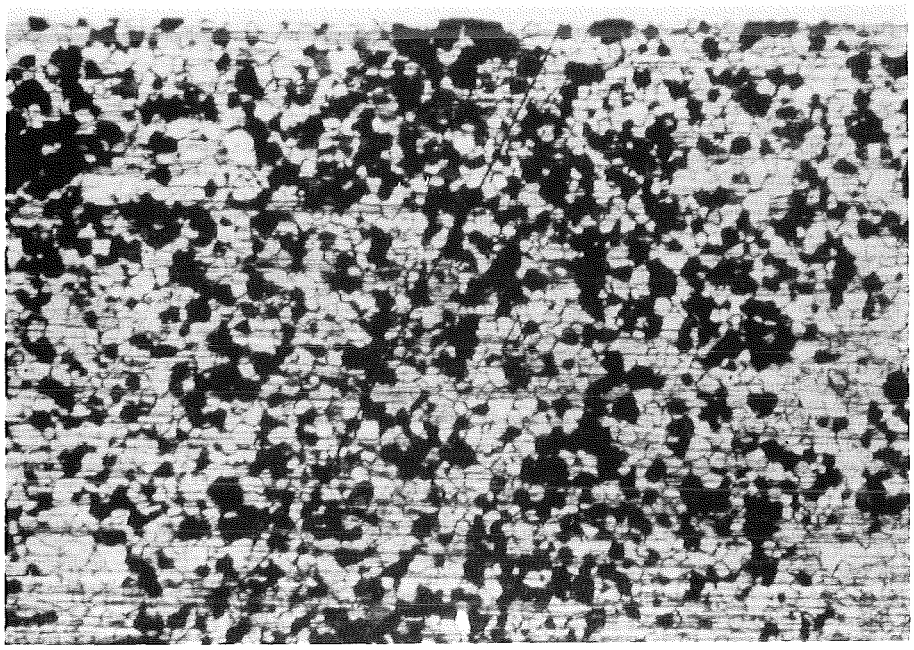

Fig. 5 Light microscopic photograph of sample No. 2 after reaction with nitrogen, magnification x 50.

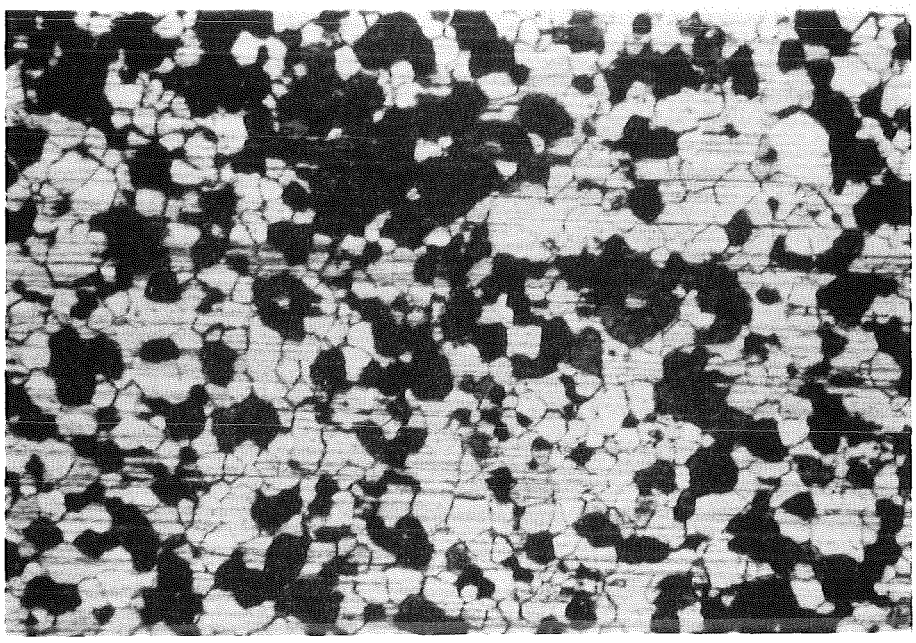

Fig. 6 Light microscopic photograph of sample No. 2 after reaction with nitrogen, magnification x 200.

Fig. 7 Light microscopic photograph of the ion bombarded area of sample No. 2 after measurement of the AES depth profile. The slightly brighter square in the center of the photograph represents the sputtered part of the surface. The dark spot in the upper left of the photograph corresponds to a mechanical damage of the surface which occurred after the depth profile measurement (magnification x 50).

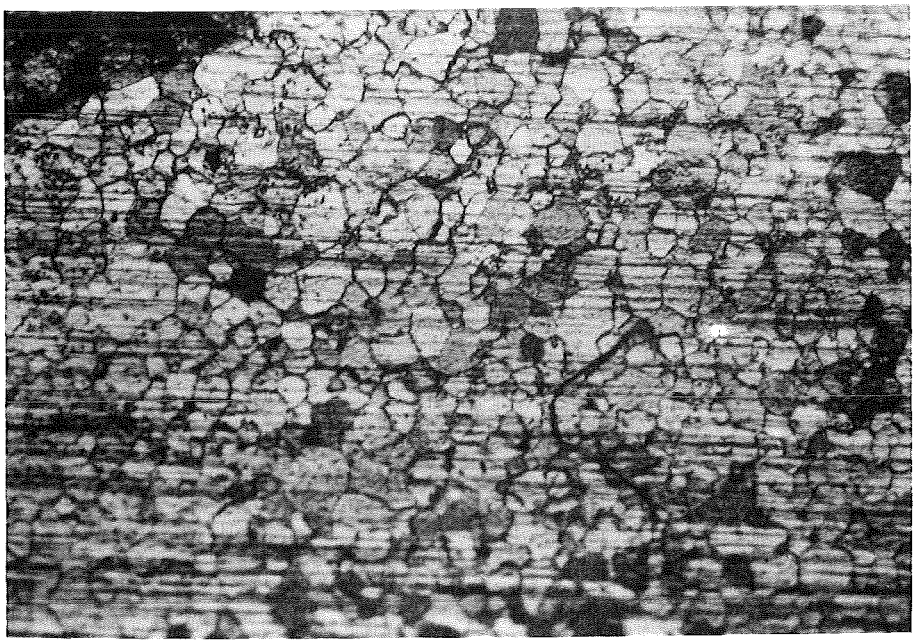

Fig. 8 Same as Fig. 7, but showing the center of the sputtered area; magnification x 100.

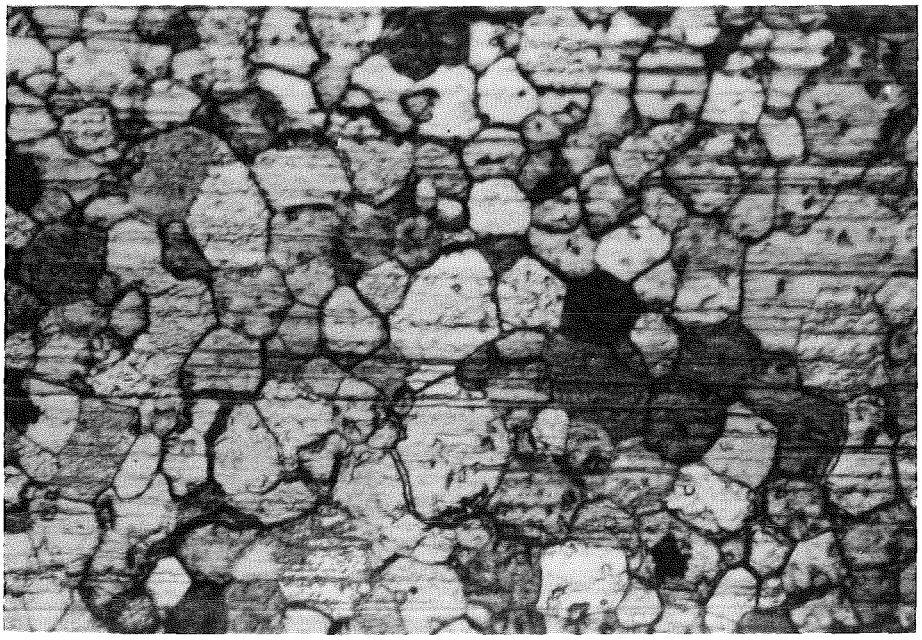

Fig. 9 Light microscopic photograph of the ion bombarded area of sample No. 2 after measurement of the AES depth profile, magnification x 200. The photograph may be compared with Fig. 13.

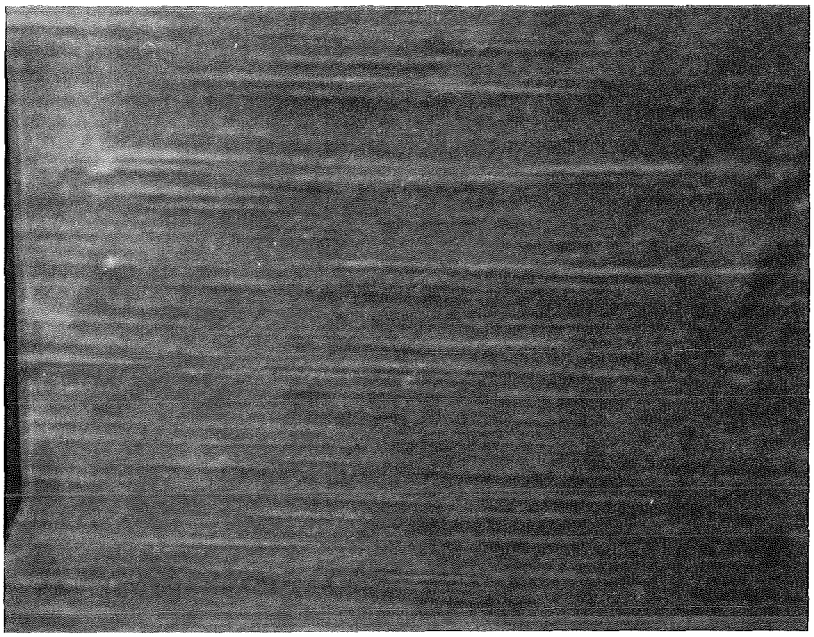

Fig. 10 SEM micrograph of sample No. 2 after reaction with nitrogen; magnification x 100.

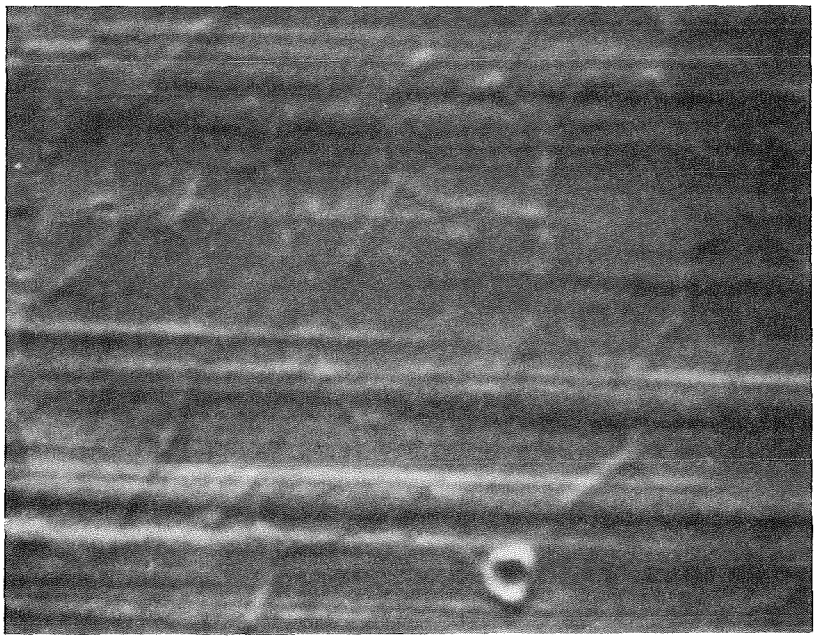

Fig. 11 SEM micrograph of sample No. 2 after reaction with nitrogen; magnification x 400.

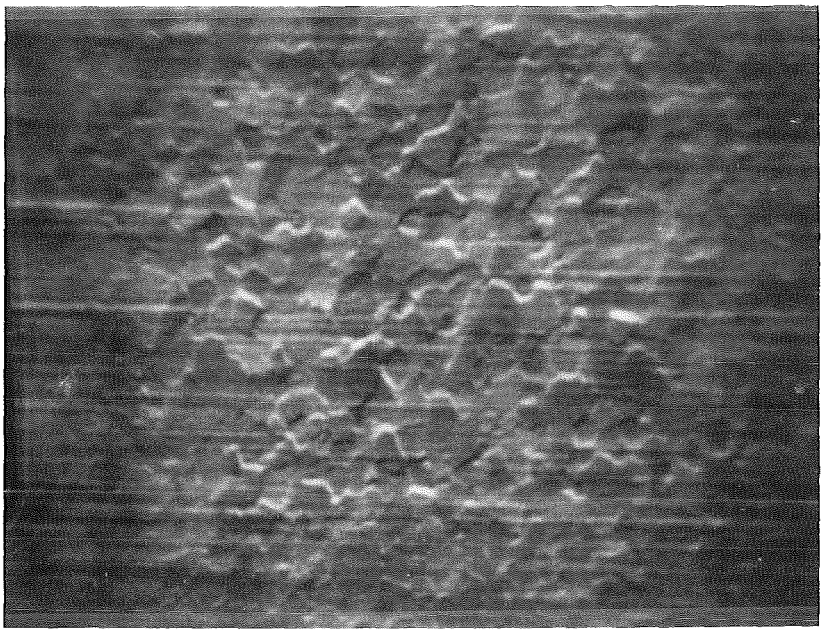

Fig. 12 SEM micrograph of sample No. 2 after reaction with nitrogen showing the surface area which has been ion bombarded during depth profiling; magnification x 100.

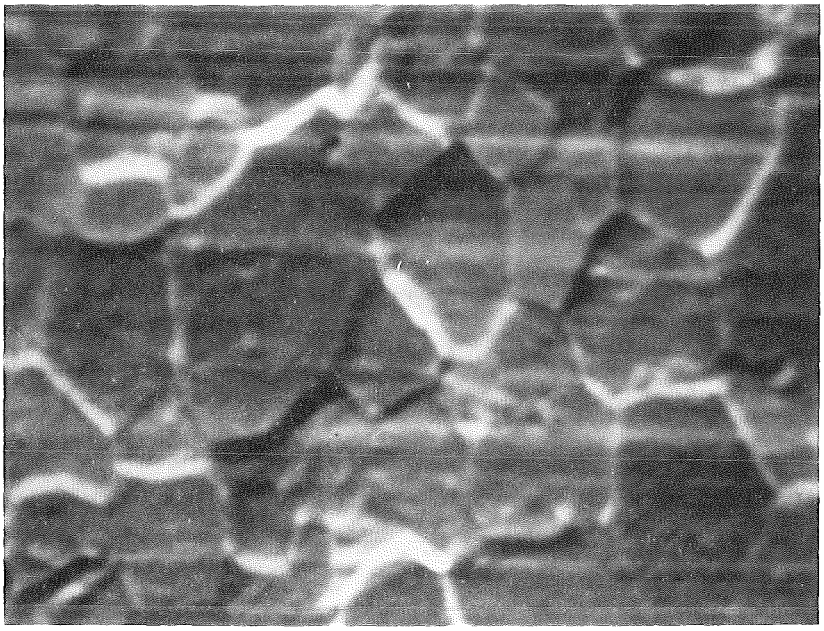

Fig. 13 SEM micrograph of sample No. 2 after reaction with nitrogen showing the surface area which has been ion bombarded during depth profiling; magnification x 400. The figure can be compared to Fig. 9.

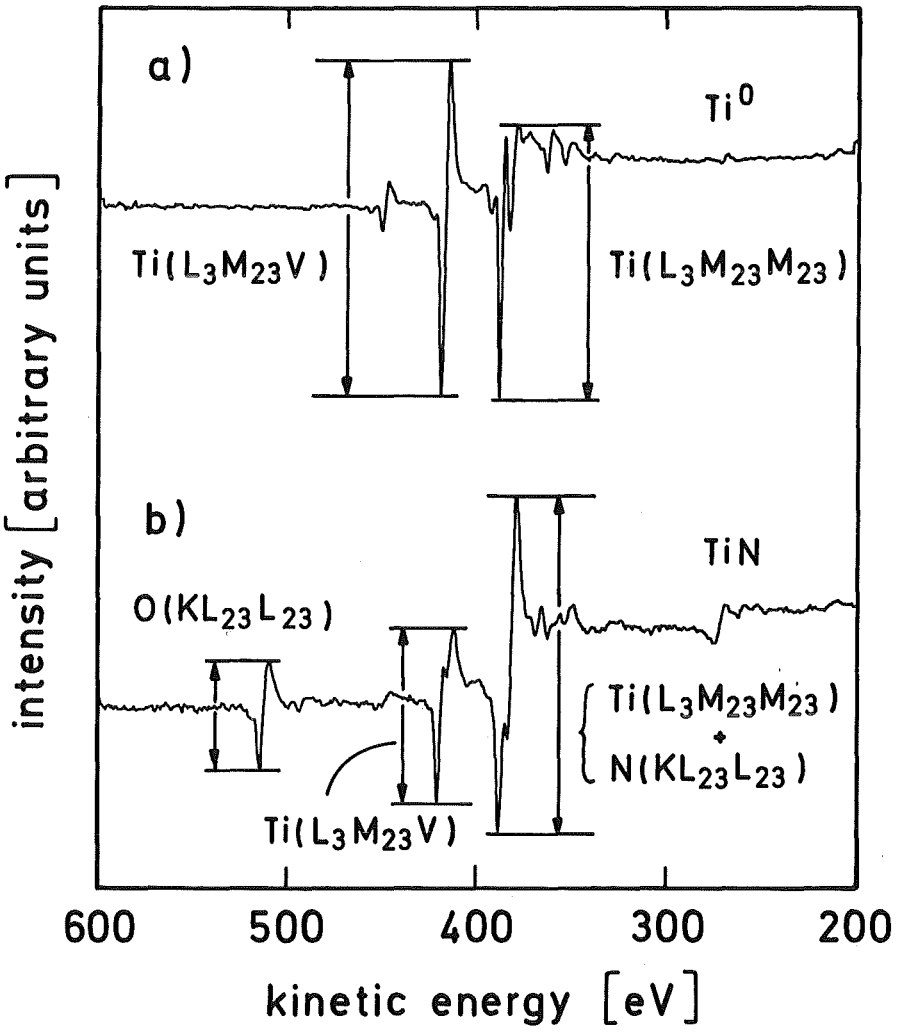

Fig. 14 AES spectra of titanium metal (a) and titanium mononitride (b). Details of the preparation and treatment of the TiN sample are given in the text. Peak heights as shown in the figure have been employed for the evaluation of depth profiles.

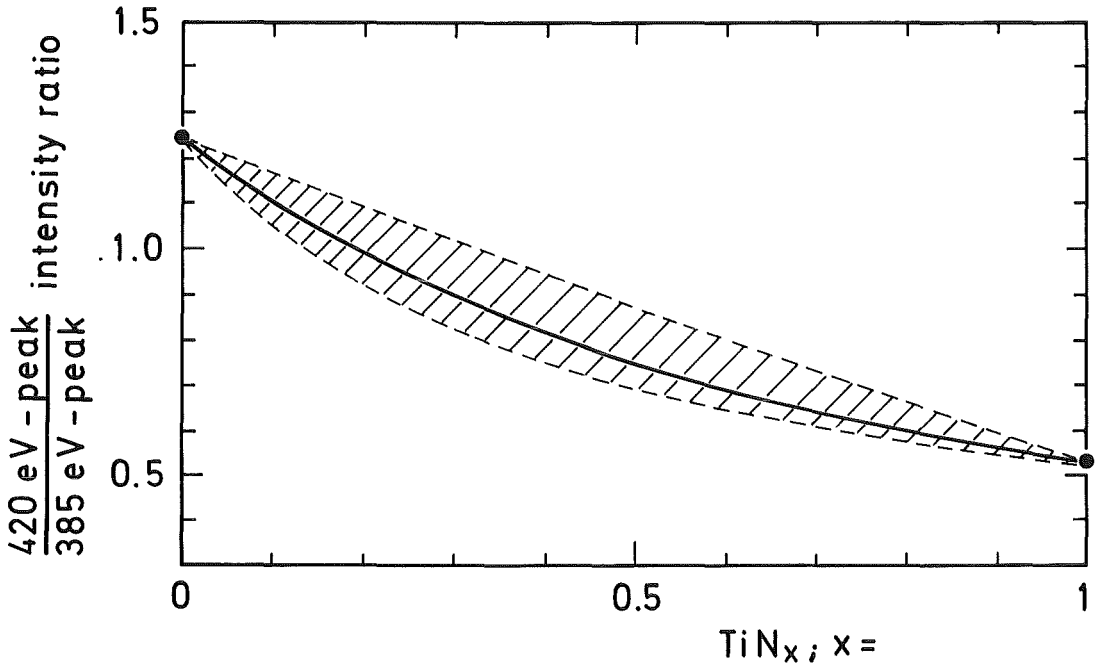

Fig. 15 Evaluation of the composition of titanium nitrides as a function of the intensity ratio of the Auger peaks at 420 eV and 385 eV kinetic energy. The plot neglects possible errors in the determination of the intensity ratios of the reference materials (x = 0 and x = 1, respectively). The continuous curve has been calculated from eq. (2) (T = 1.24; N = 0.52 and C = 0.9). The dashed lines were obtained with C values of 1.35 and 0.45, respectively, representing a 50 % deviation from the assumed true value of C of 0.9.

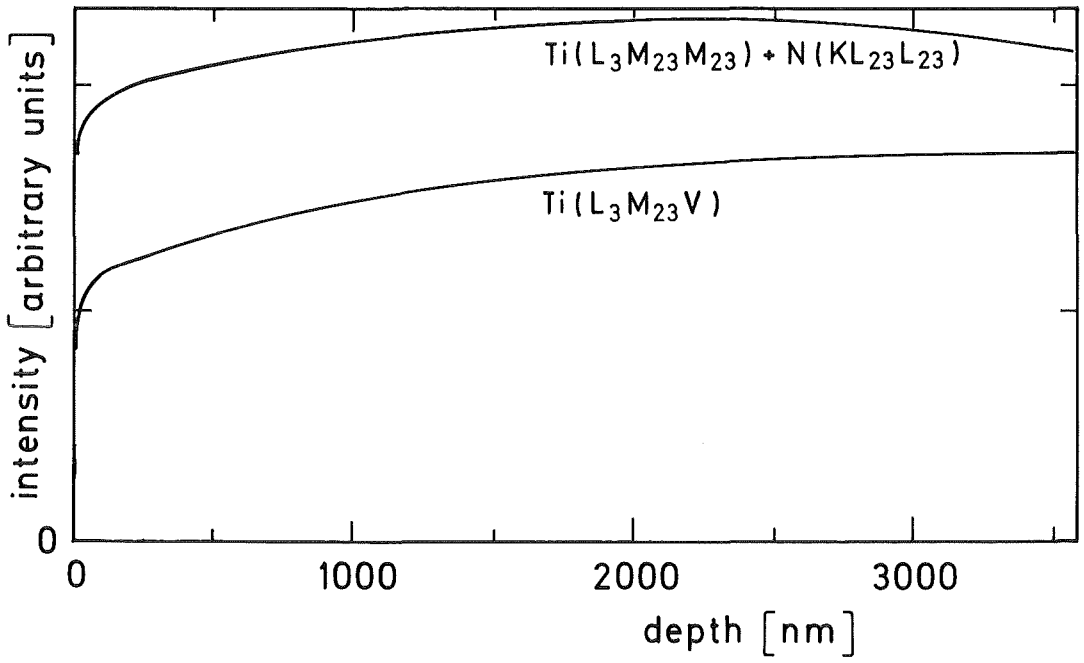

Fig. 16 a Depth profile of sample No. 1.

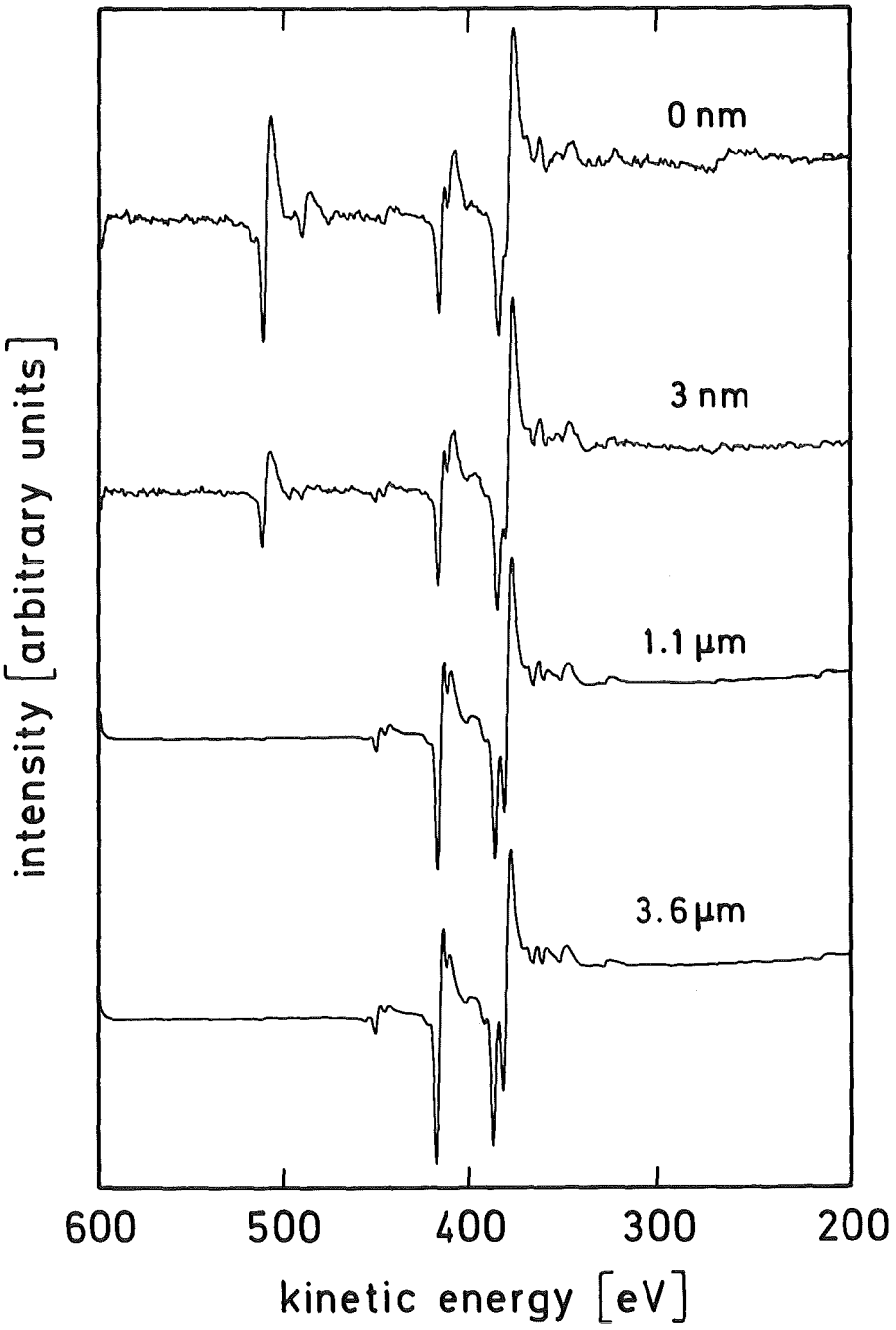

Fig. 16 b Auger spectra of sample No. 1 corresponding to selected depths of the data shown in Fig. 16 a.

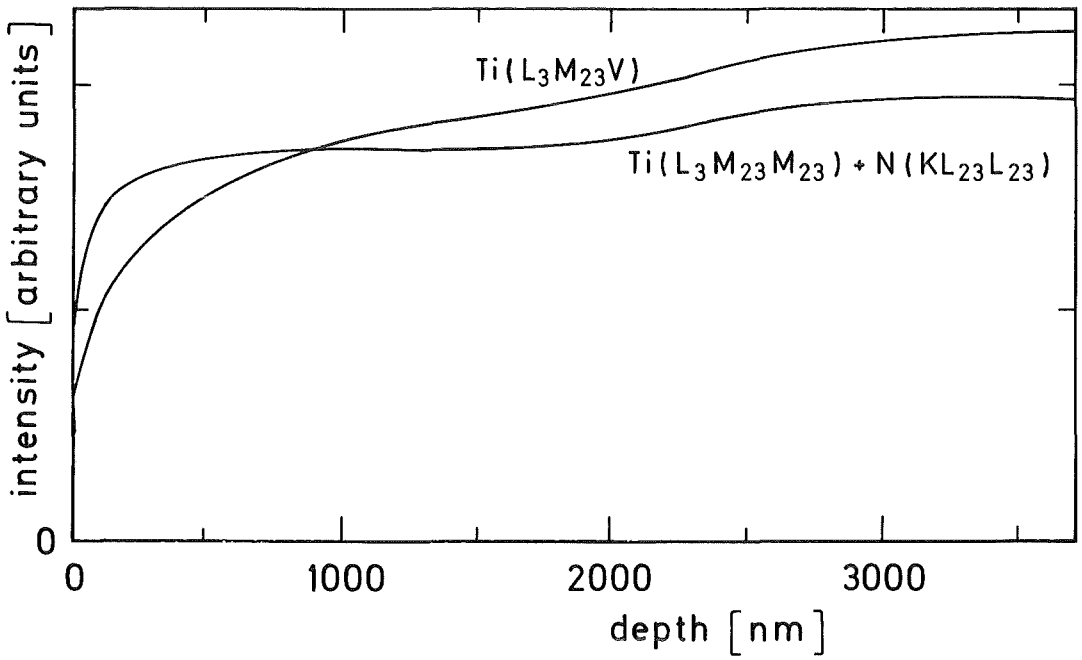

Fig. 17 a Depth profile of sample No. 2.

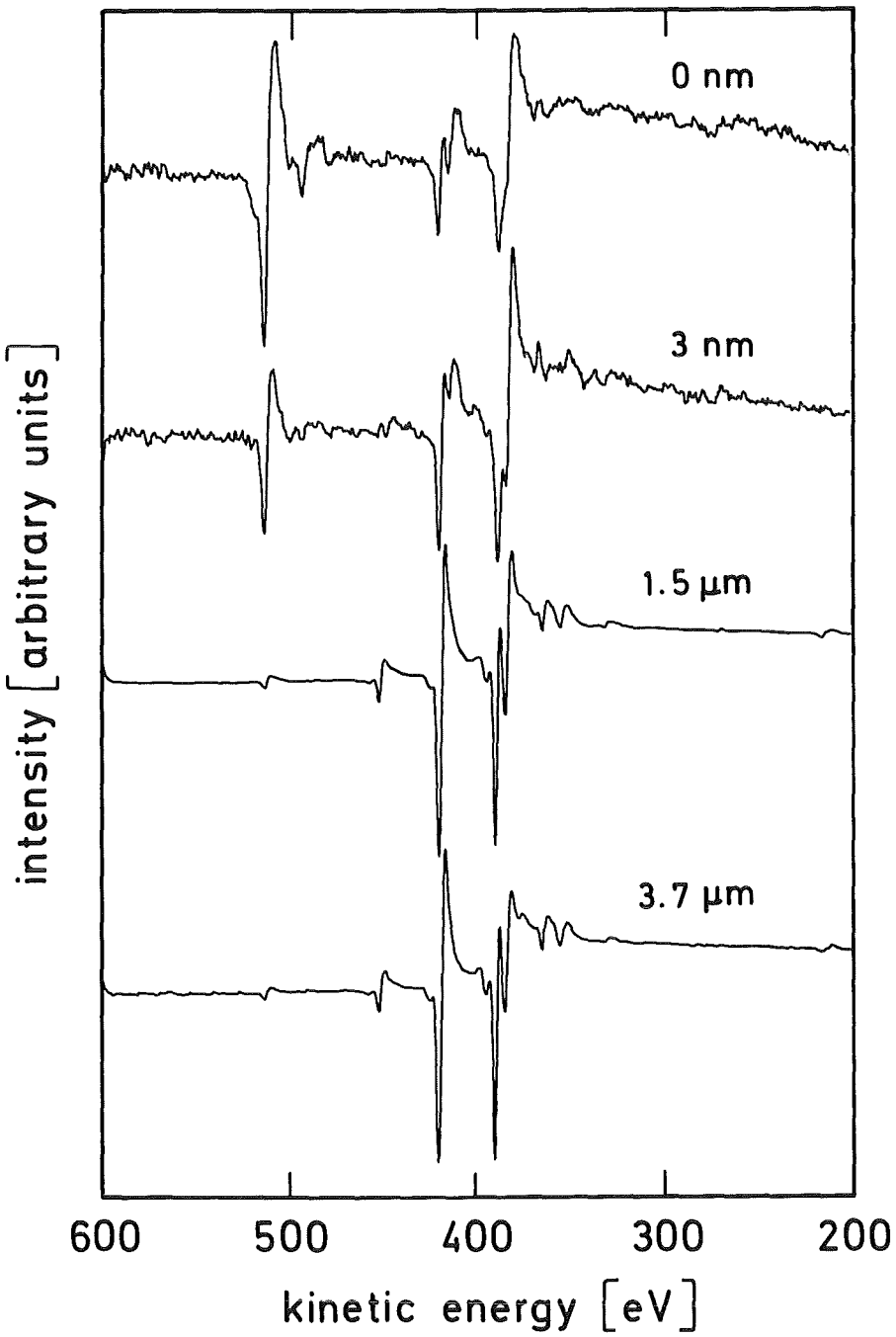

Fig. 17 b Auger spectra of sample No. 2 corresponding to selected depths of the data shown in Fig. 17 a.

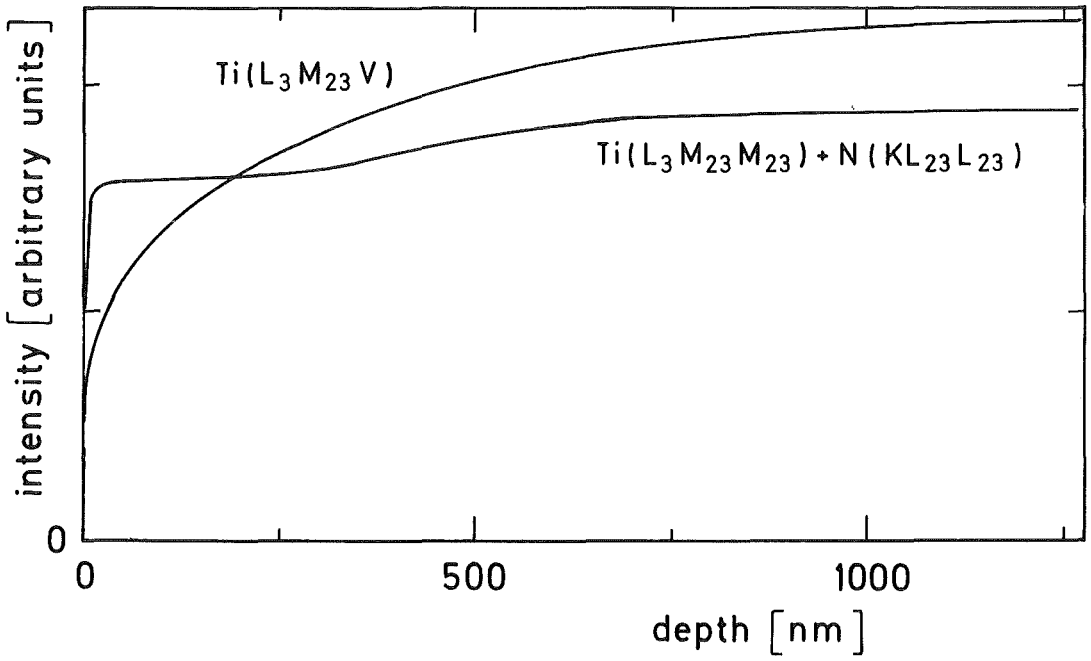

Fig. 18 a Depth profile of sample No. 3.

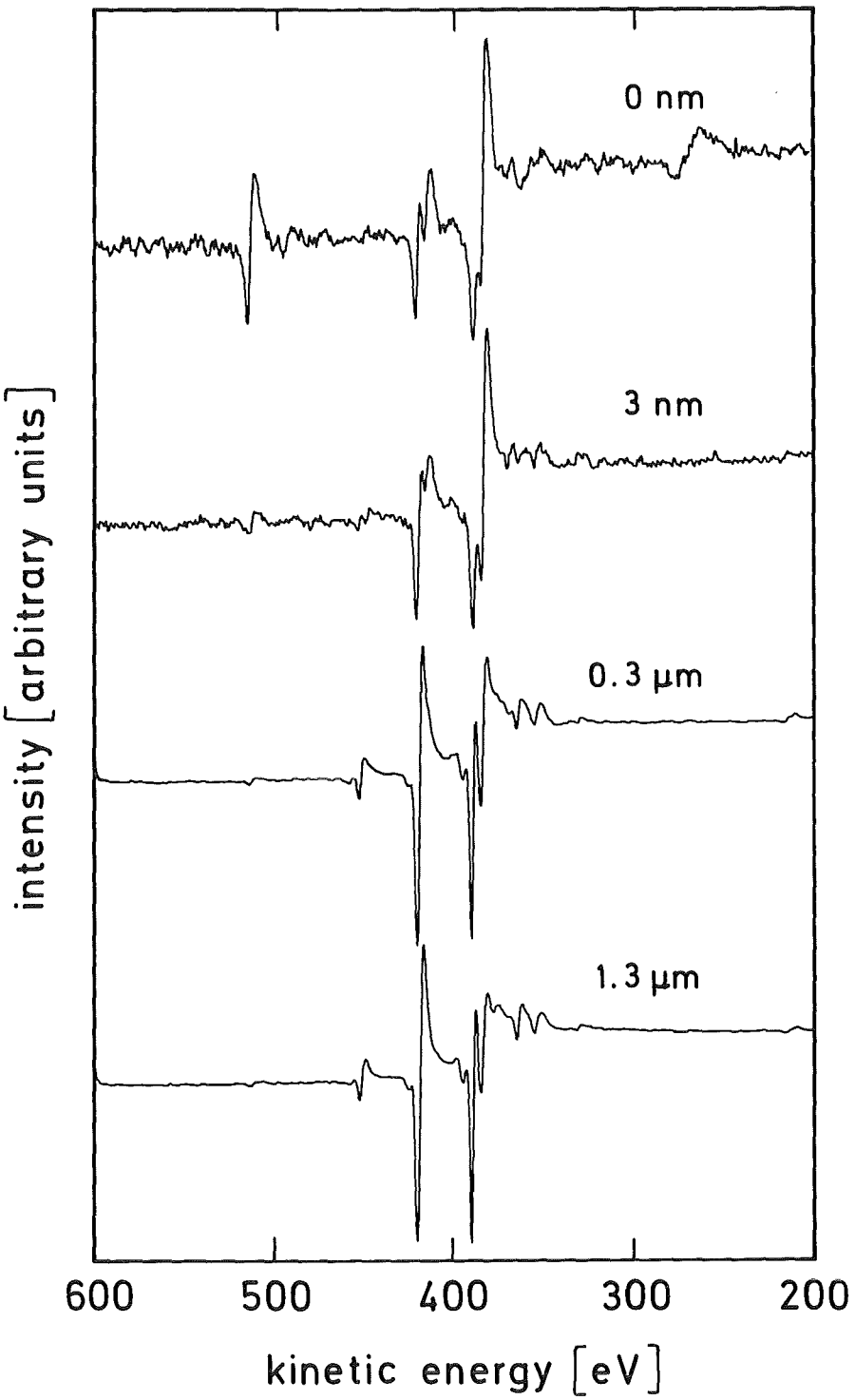

Fig. 18 b Auger spectra of sample No. 3 corresponding to selected depths of the data shown in Fig. 18 a.

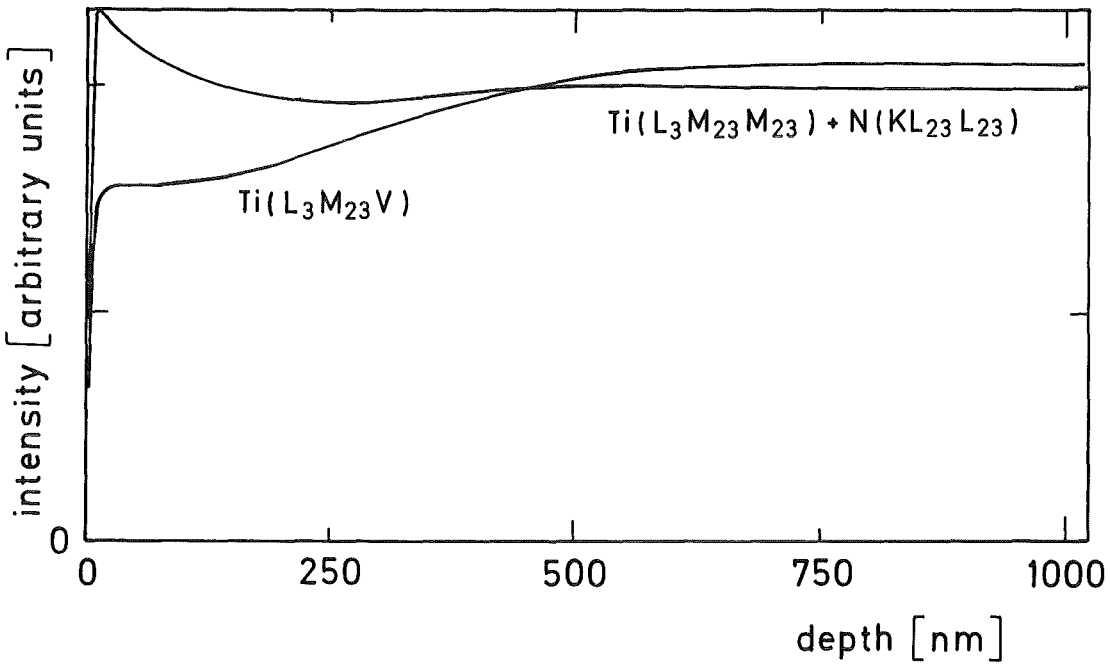

Fig. 19 a Depth profile of sample No. 4.

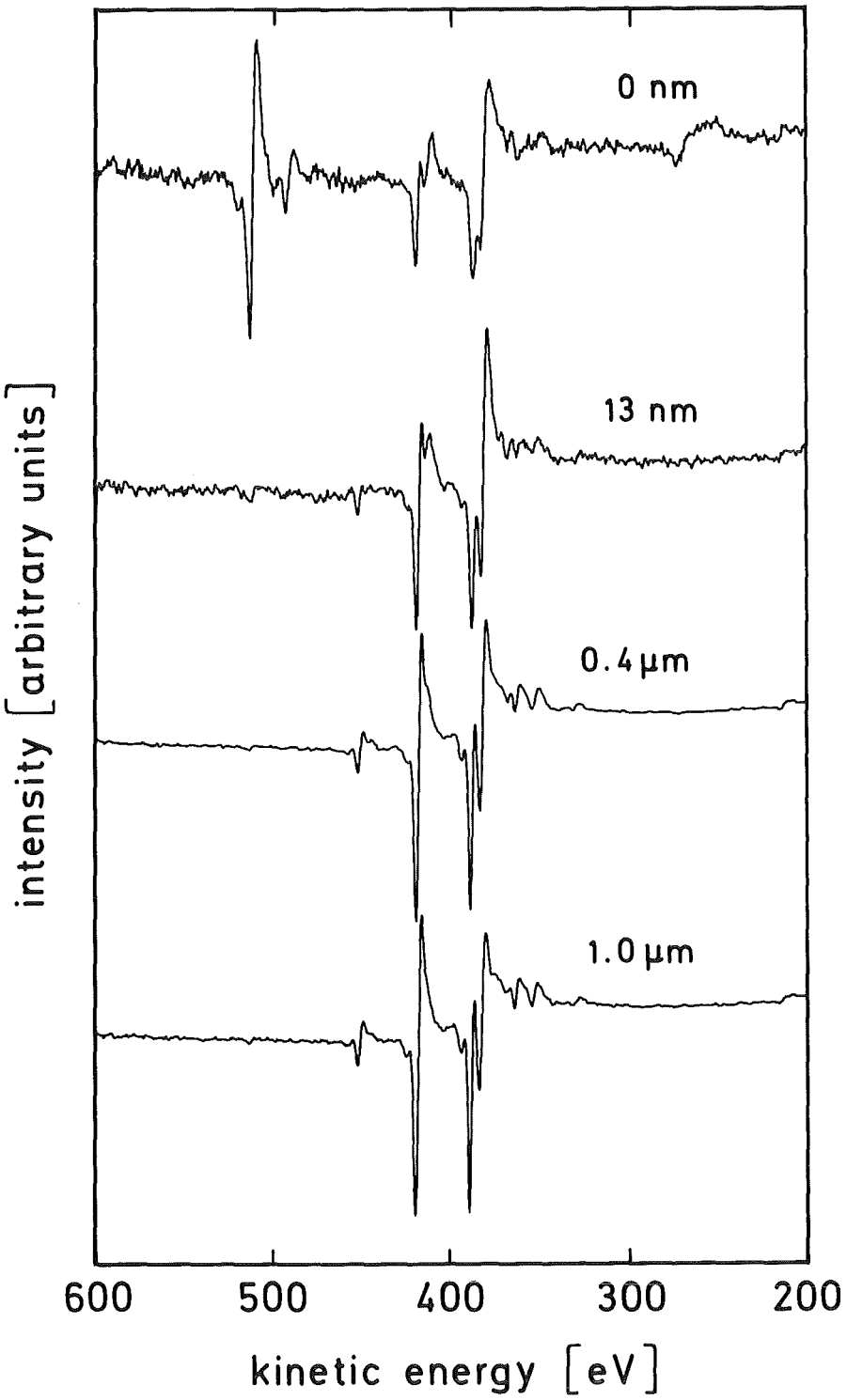

Fig. 19 b Auger spectra of sample No. 4 corresponding to selected depths of the data shown in Fig. 19 a.

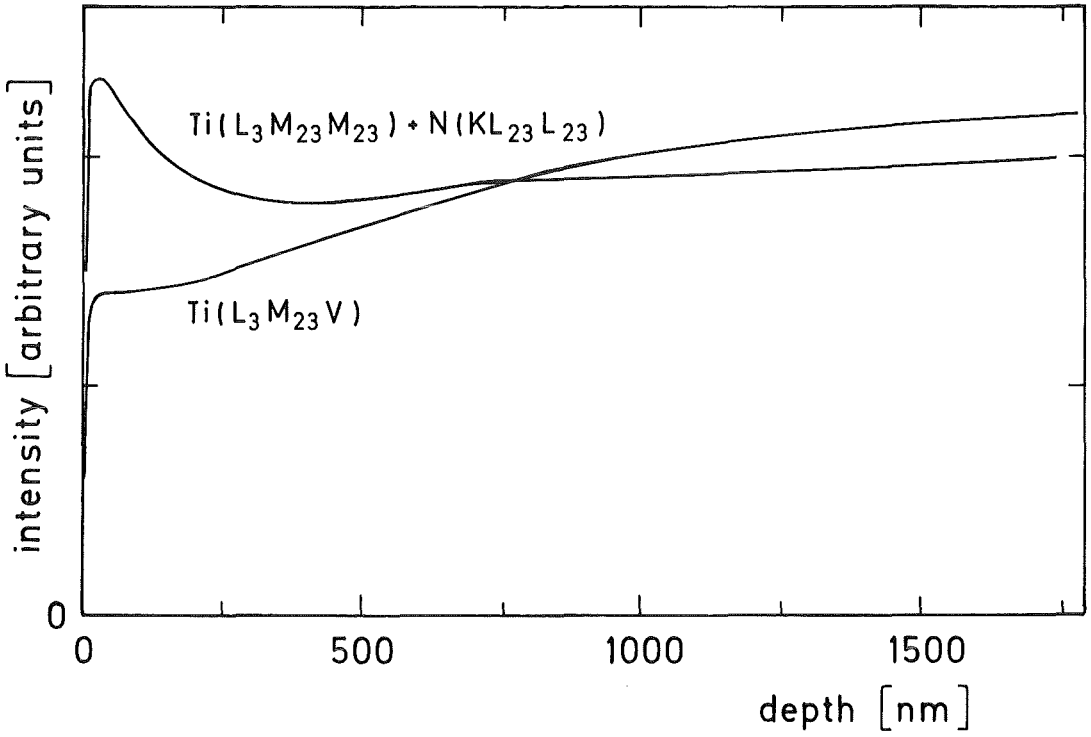

Fig. 20 a Depth profile of sample No. 5.

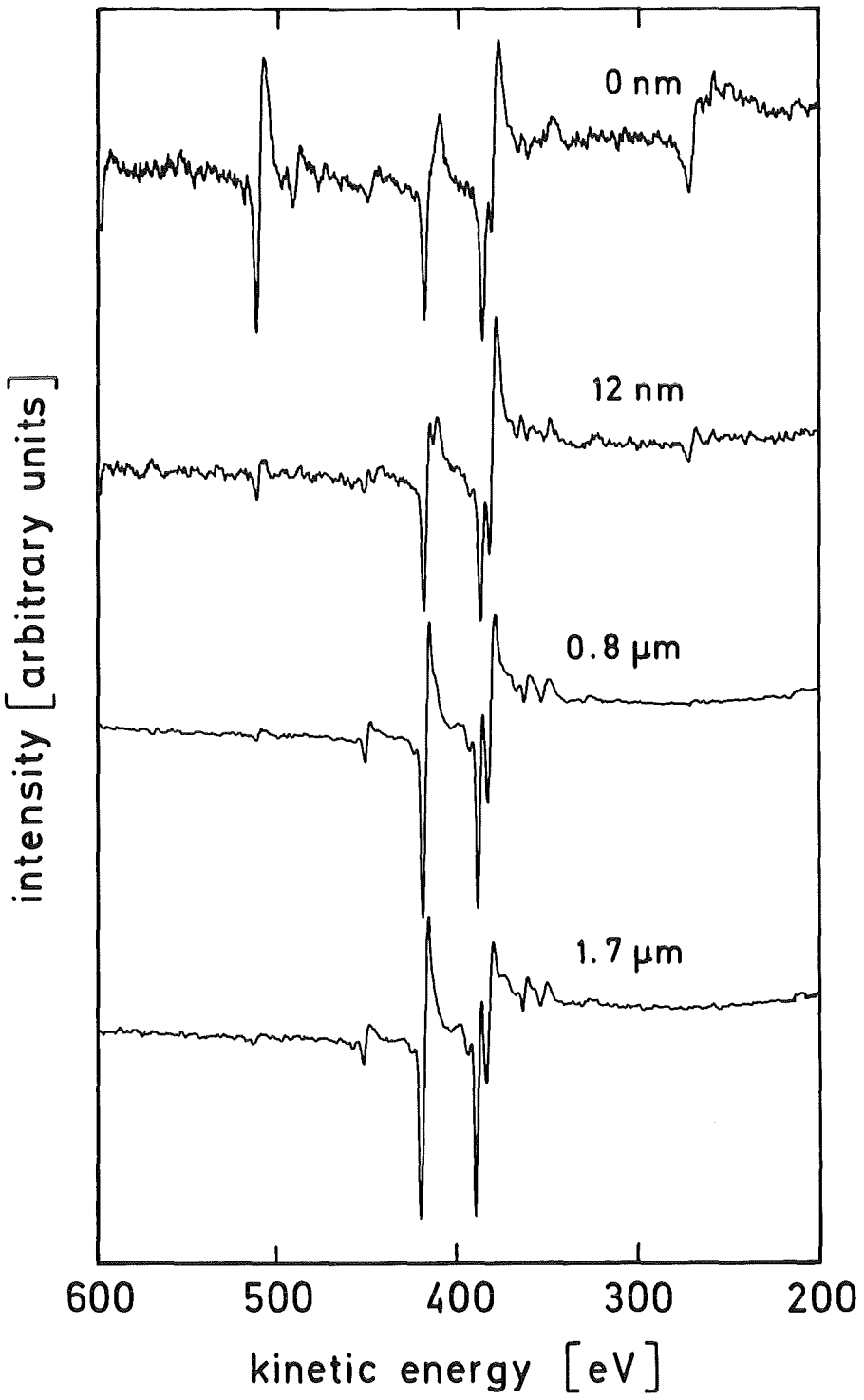

Fig. 20 b Auger spectra of sample No. 5 corresponding to selected depths of the data shown in Fig. 20 a.

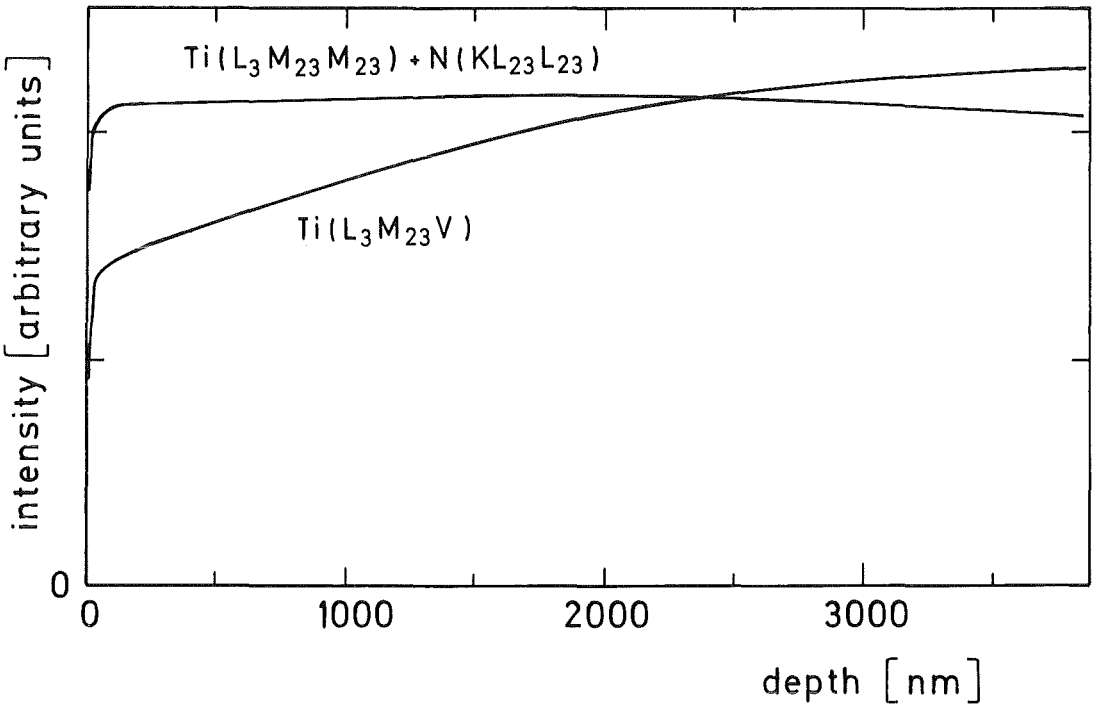

Fig. 21 a Depth profile of sample No. 6.

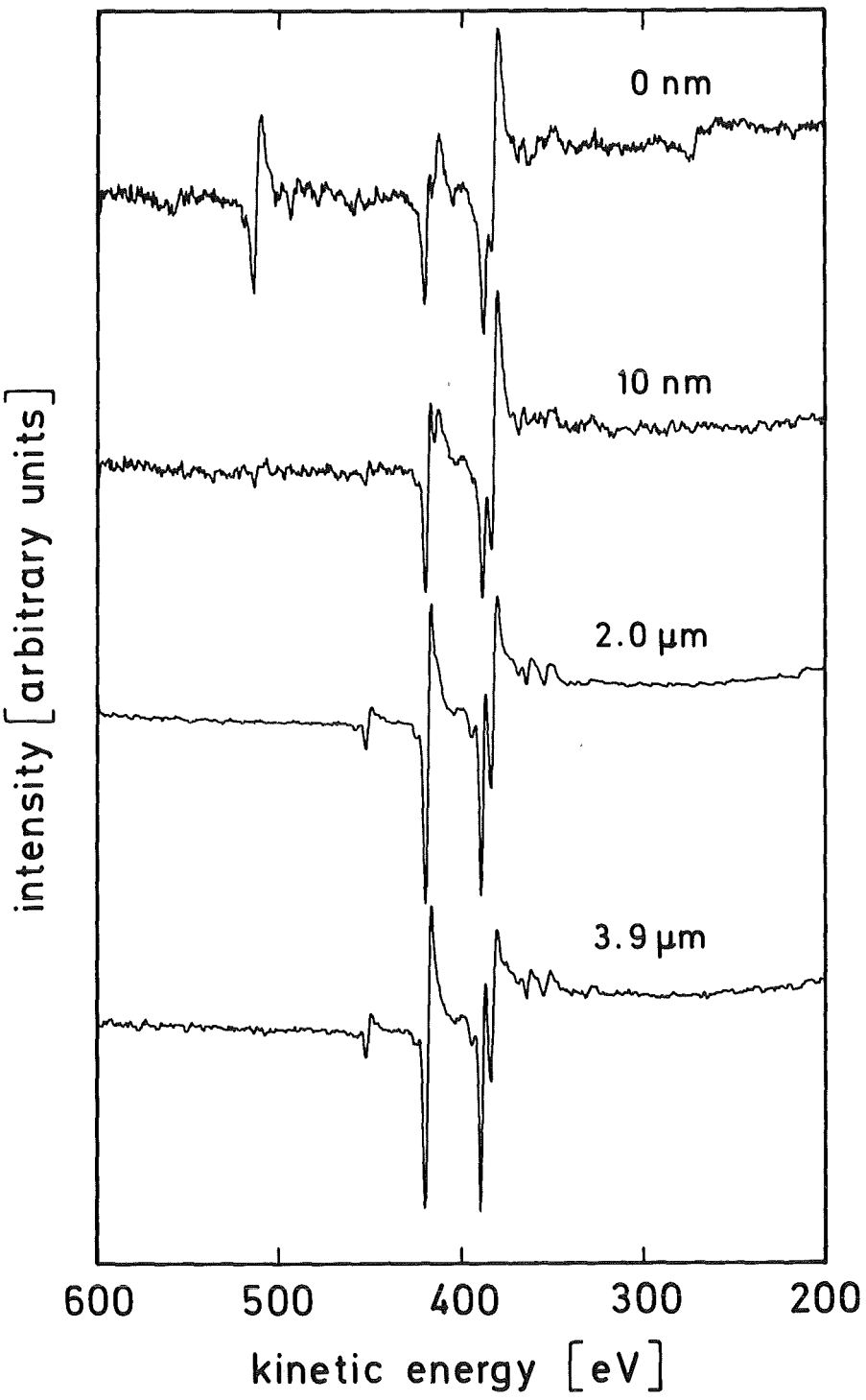

Fig. 21 b Auger spectra of sample No. 6 corresponding to selected depths of the data shown in Fig. 21 a.

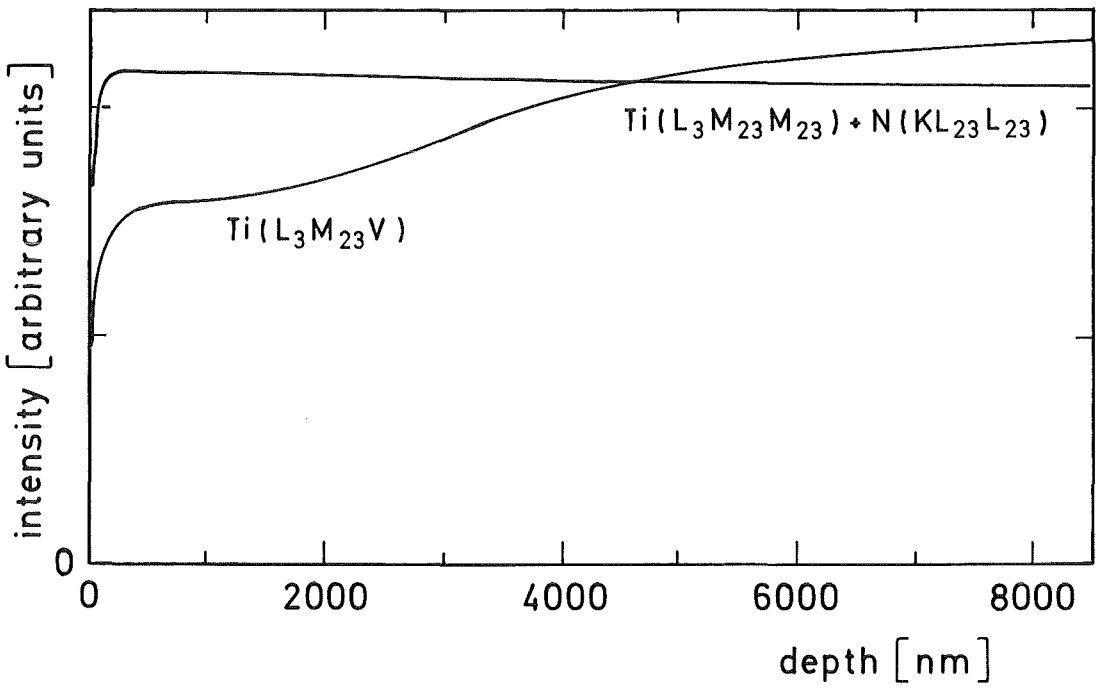

Fig. 22 a Depth profile of sample No. 7.

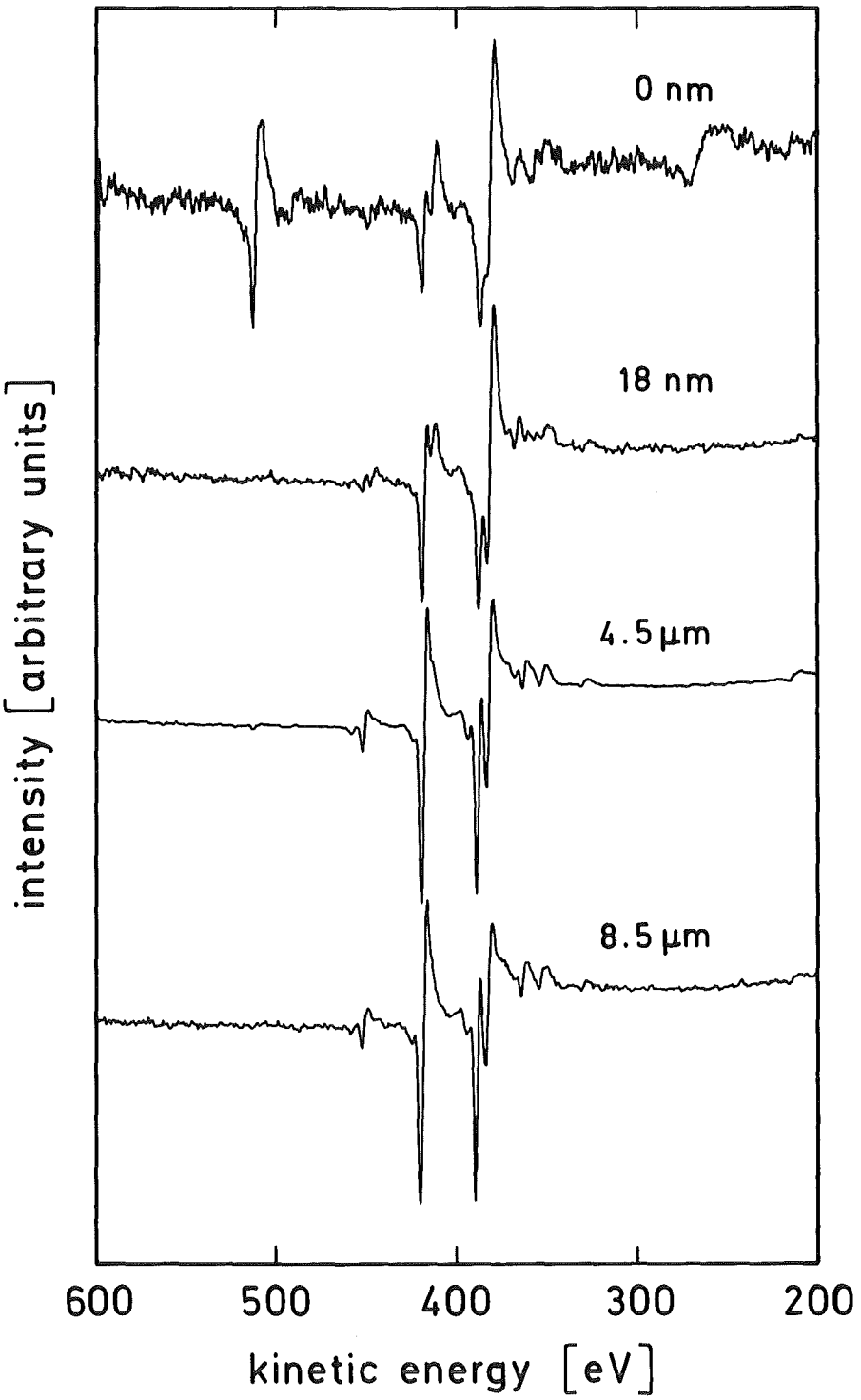

Fig. 22 b Auger spectra of sample No. 7 corresponding to selected depths of the data shown in Fig. 22 a.

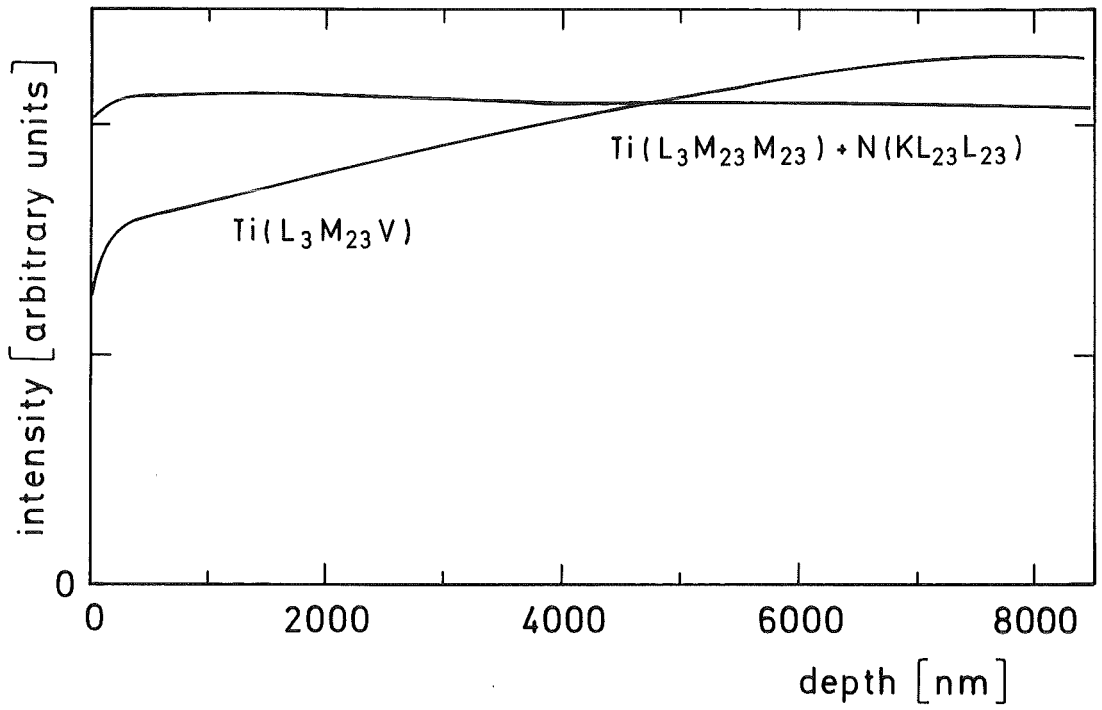

Fig. 23 a Depth profile of sample No. 8.

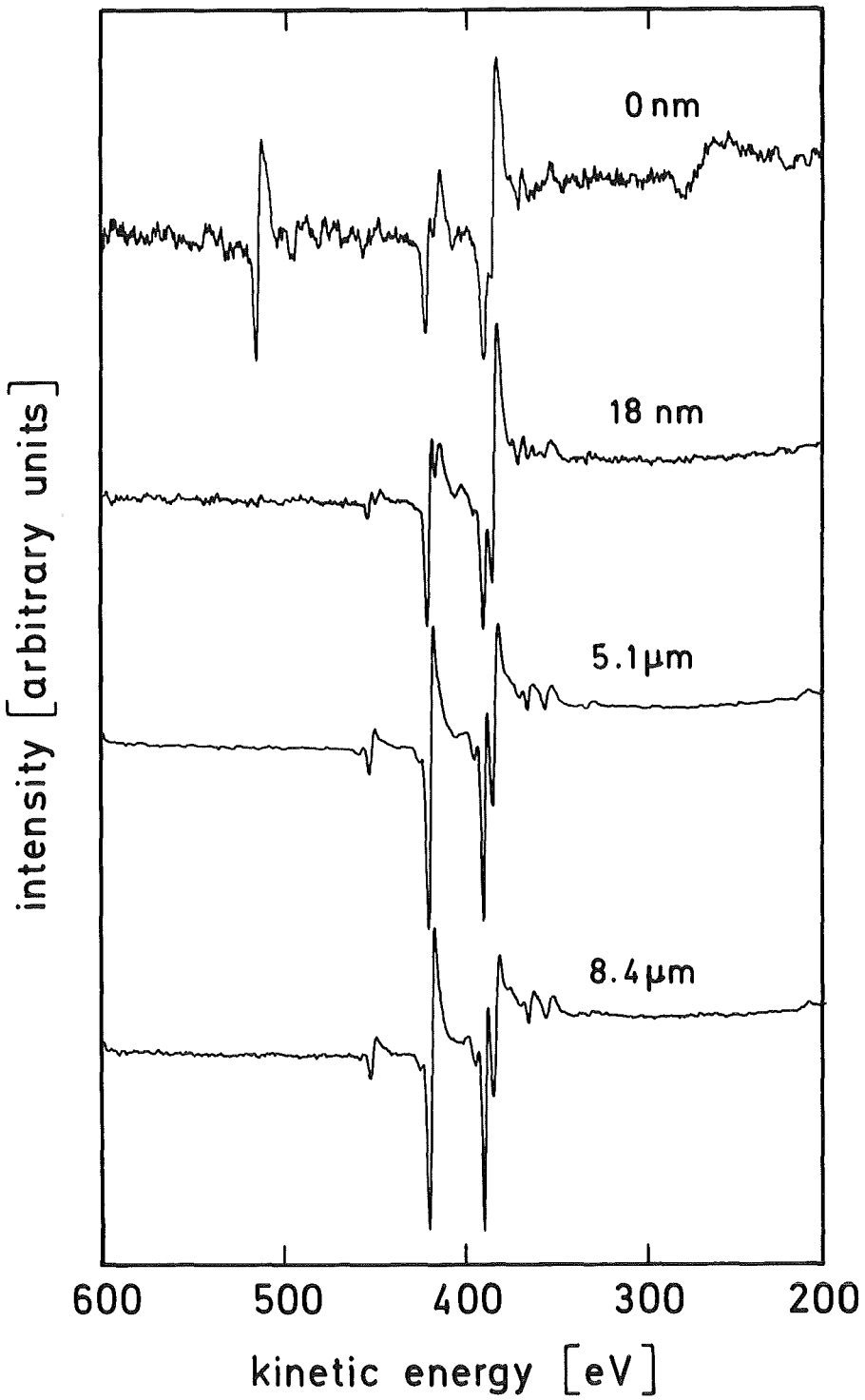

Fig. 23 b Auger spectra of sample No. 8 corresponding to selected depths of the data shown in Fig. 23 a.

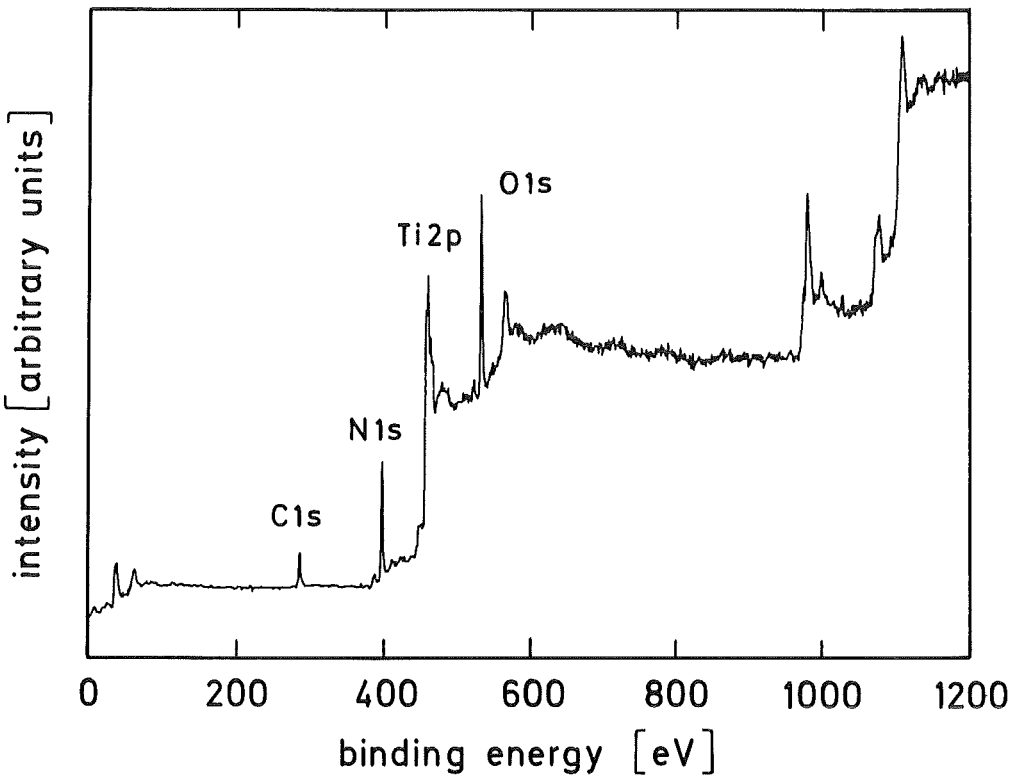

Fig. 24 XPS spectrum of sample No. 7 showing the major photoelectron transitions obtained with Al K_α radiation.

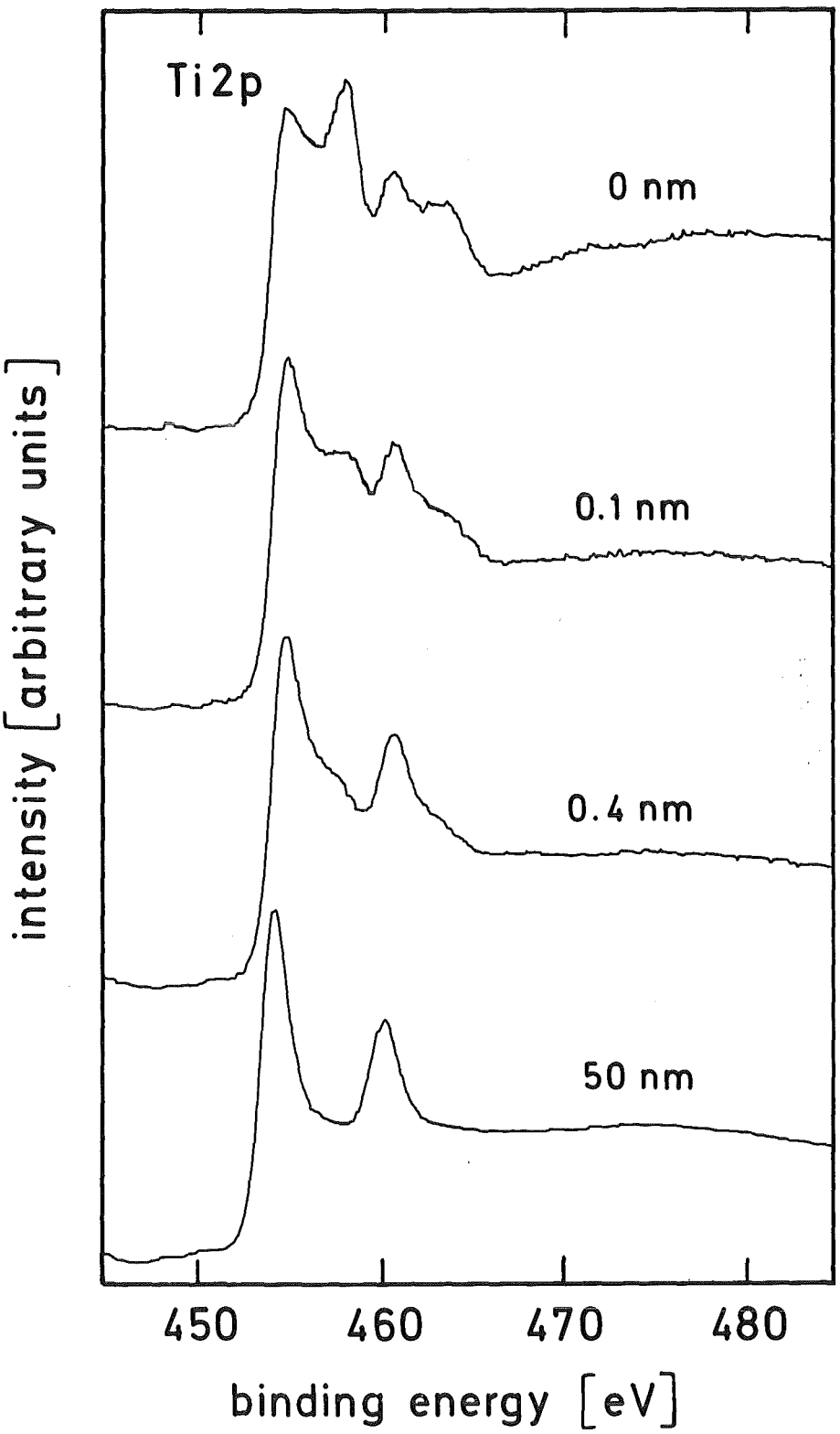

Fig. 25 Ti 2p XPS spectra of sample No. 3 at various depths using the Al K_α radiation. Depth values were calculated from the employed ion current density. Particularly in the zone close to the surface they are very uncertain due to the unavailability of reliable sputtering rates.

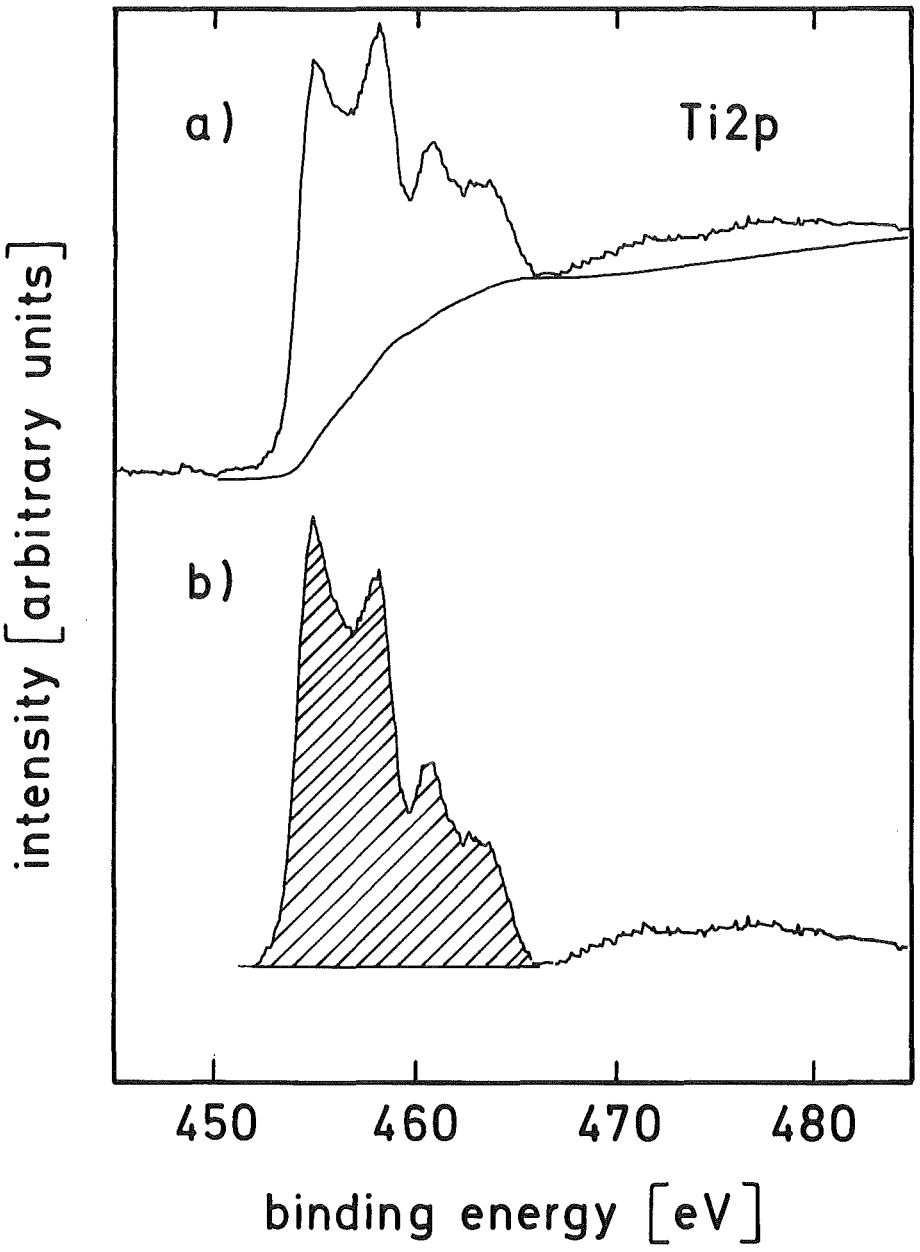

Fig. 26 Ti 2p XPS spectrum of sample No. 3 (surface composition): a) raw spectrum and background caused by inelastically scattered electrons; b) spectrum after subtraction of background and X-ray satellites. The hatched peak area corresponds to the intensity of the photoemission.

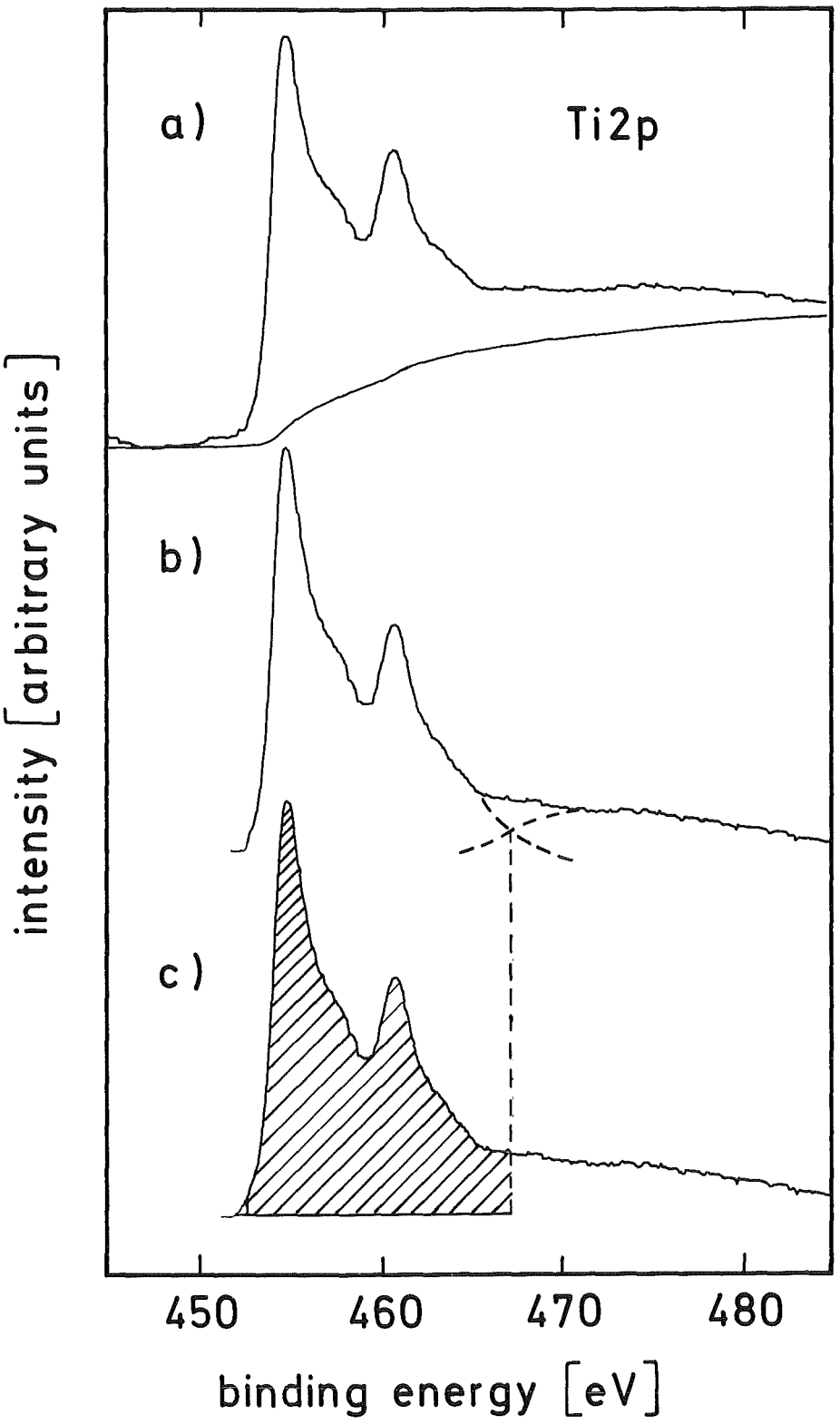

Fig. 27 Ti 2p XPS spectrum of sample No. 3 (nominal depth 0.4 nm): a) raw spectrum and background caused by inelastically scattered electrons; b) spectrum after subtraction of background and X-ray satellites. The dashed lines indicate the expected courses of the photopeak multiplet and the plasmon distribution, respectively. The position of the intersect corresponds to the binding energy at the minimum in Fig. 26 b; c) equivalent to b, the hatched peak area corresponds to the intensity of the photoemission.

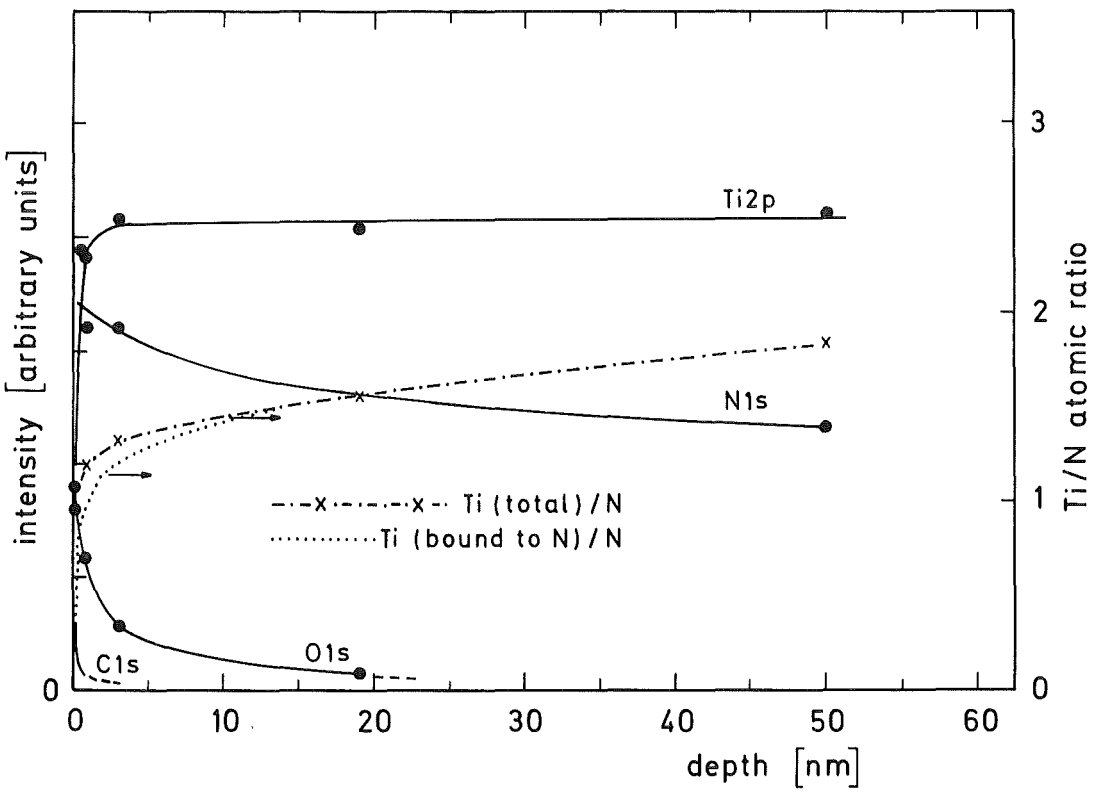

Fig. 28 Depth profile of sample No. 3 evaluated from XPS measurements. The intensities of the photopeaks are displayed on the left ordinate (continuous curves) and the atomic Ti/N ratios are shown on the right ordinate. -·- x -·- gives the total amount of titanium to nitrogen and ····· gives the atomic titanium/nitrogen ratio after correction for the titanium fraction bound to oxygen. This fraction was calculated from the oxygen signal intensity under the assumption of an average stoichiometry of $TiO_{1.5}$.

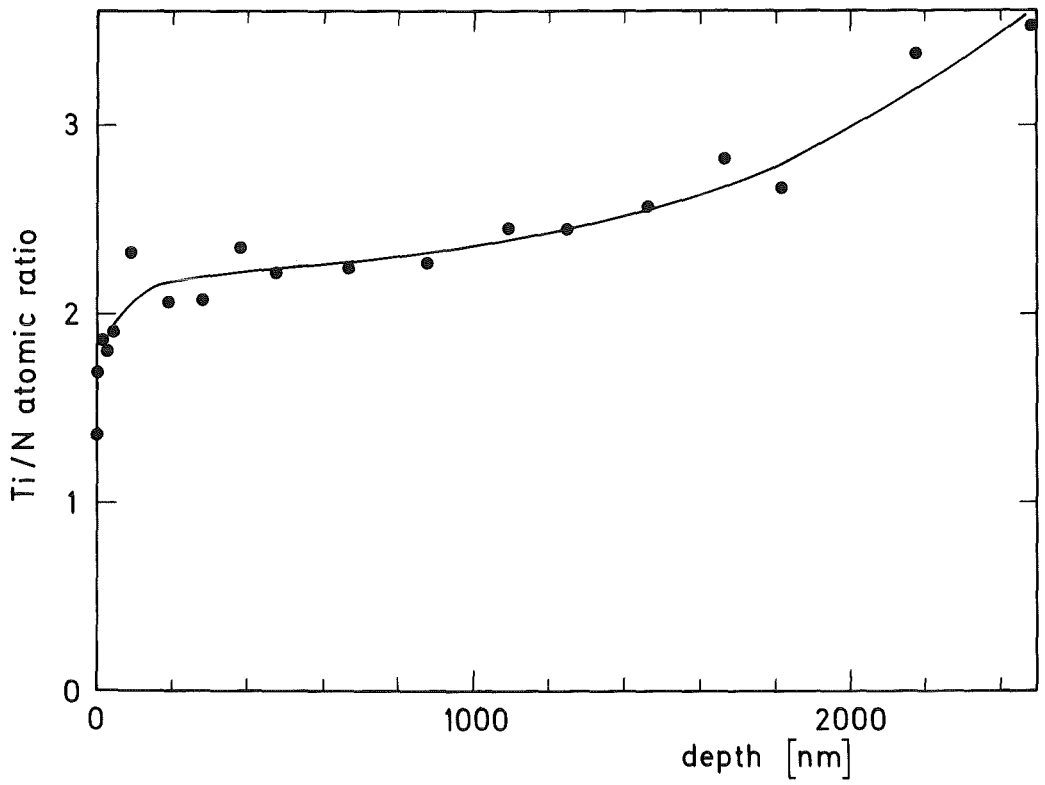

Fig. 29 Depth profile of the titanium to nitrogen atomic ratio of sample No. 7 evaluated from XPS measurements.

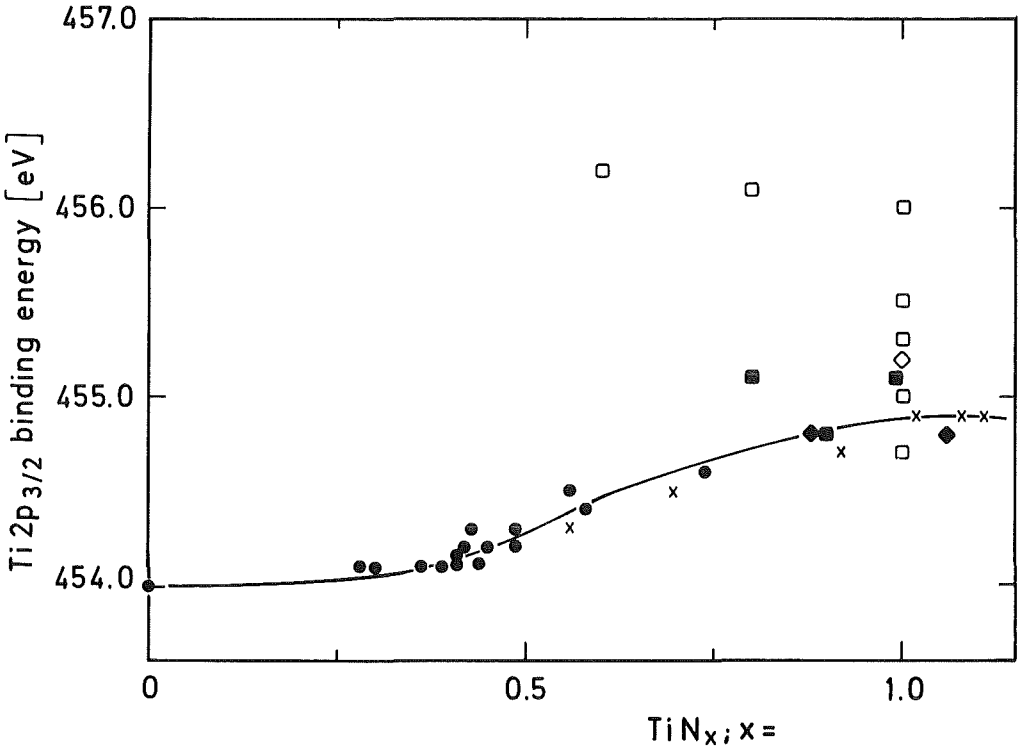

Fig. 30 Correlation between the Ti $2p_{3/2}$ binding energy and the composition of the titanium nitride TiN_x (● from XPS depth profile measurements with sample No. 7; x from XPS depth profile measurements with sample No. 3; ◇ from TiN_1 powder before sputtering; ◆ from TiN_1 powder after sputtering; □ literature values evaluated from samples having a partially oxidized surface, and ■ literature values evaluated from samples having a clean or a cleaned surface (for literature values see Table 6). Values of $x \geqslant 1$ are acceptable because the TiN_x phase has been observed to exist up to x-values of 1.16 (9).

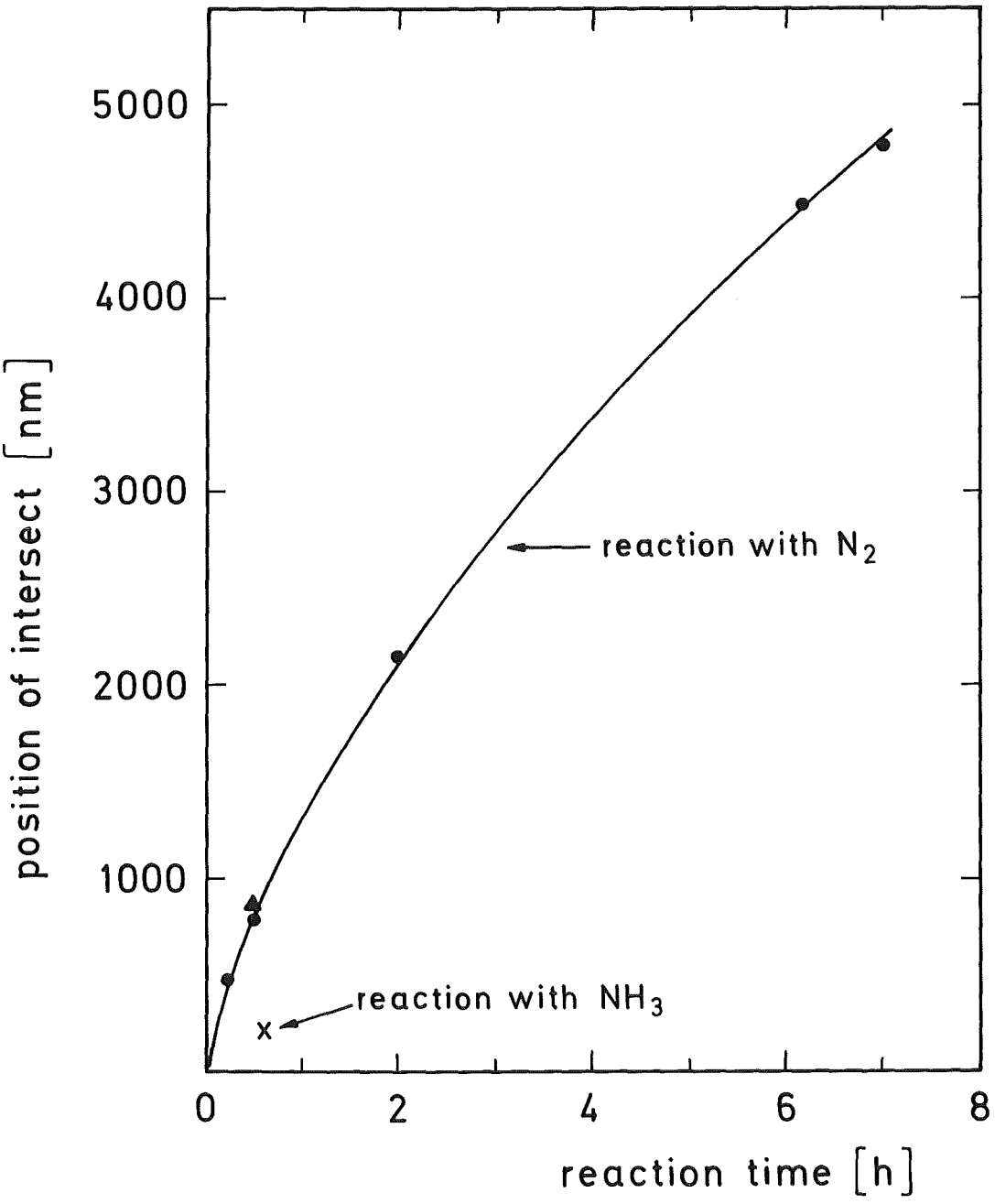

Fig. 31 Position of the point of intersect as a function of reaction time at 890 °C (● samples 4-8; ▲ sample 2, x sample 3).

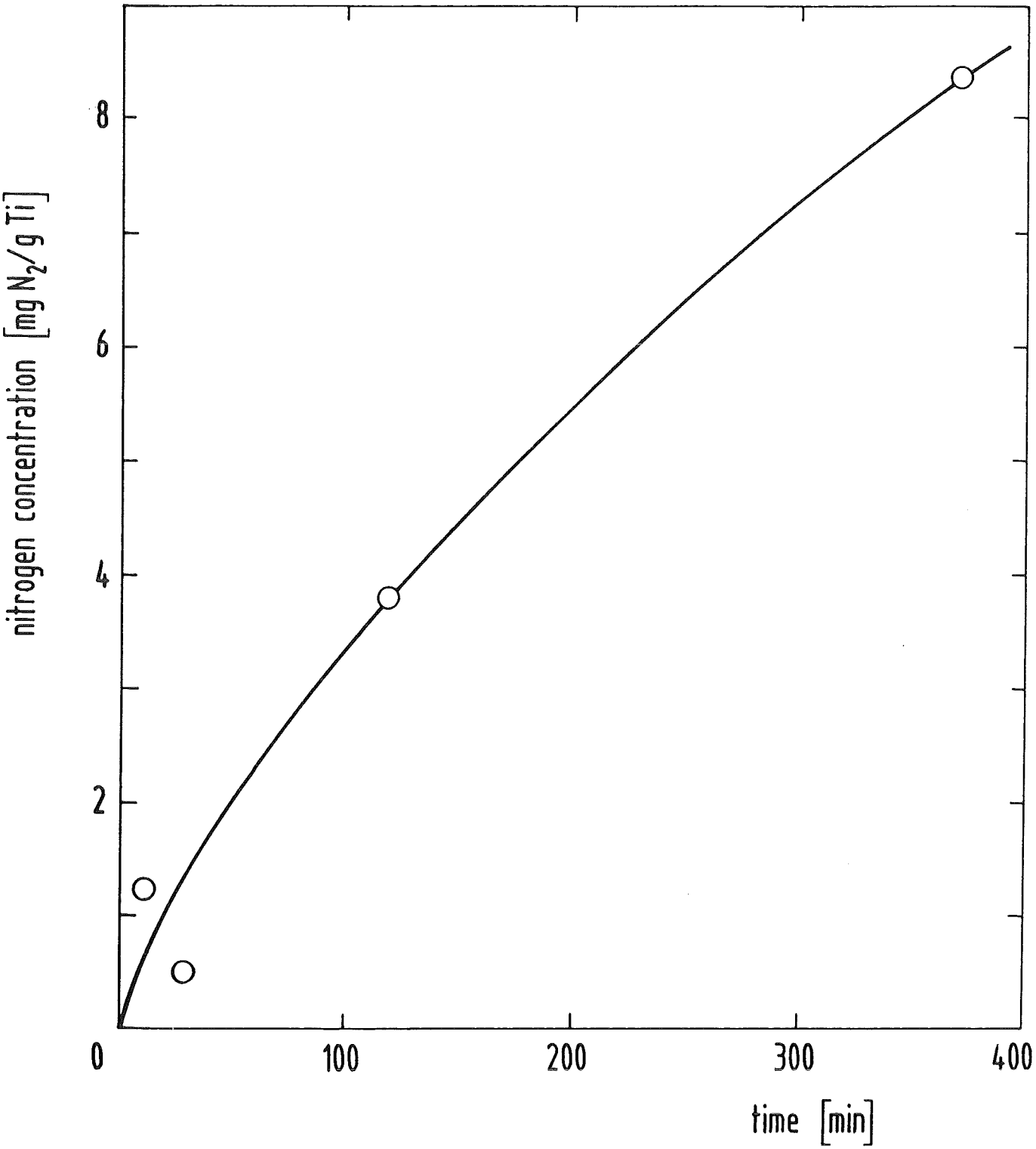

Fig. 32 Volumetric determination of the nitrogen uptake by titanium foils at 890 °C as a function of time (see Table 8).

Literature

1. J.O. Noga, Ontario Hydro Research Division, Report Nr. 81-368 K (1981).
2. J.M. Yaraskavitch, W.J. Holtslander, Proc. Miami Int. Symp. on Metal-Hydrogen Systems, p. 619 (1981).
3. N.P. Kherani, W.T. Shmayda, Fusion Technol. 8, 2399 (1985).
4. E.C. Kerr, J.R. Bartlit, R.H. Sherman, Proc. Tritium Technol. in Fission, Fusion and Isotope Application, Dayton, Ohio, p. 115, April (1980).
5. L. Ramqvist, K. Hamrin, G. Johannsson, A. Fahlman, C. Nordling, J. Phys. Chem. Solids 30, 1835 (1969).
6. Yu. M. Shul'ga, V.N. Troitskii, M.I. Aivazov, Yu. G. Borod'ko, Russ. J. Inorg. Chem. 21, 1441 (1976).
7. M. Miyagi, Y. Sato, T. Mizuno, S. Sawada, Titanium 80 - Science and Technology, Proc. 4th Int. Conf. on Titanium, Vol. 4, p. 2867, Kyoto, Japan, May 19-22 (1980).
8. L.I. Johansson, P.M. Stefan, M.L. Shek, A. Nordlund Christensen, Phys. Rev. B22, 1032 (1980).
9. P.T. Dawson, S.A.J. Stazyk, J. Vac. Sci. Technol. 21, 36 (1982).
10. P.T. Dawson, S.A.J. Stazyk, J. Vac. Sci. Technol. 20, 966 (1982).
11. H. Höchst, R.D. Bringans, P. Steiner, Th. Wolf, Phys. Rev. B25, 7183 (1982).
12. N. Van Hieu, D. Lichtman, Appl. Surf. Sci. 20, 186 (1984).
13. P.T. Dawson, K.K. Tzatzov, Surf. Sci. 149, 105 (1985).
14. P.T. Dawson, K.K. Tzatzov, Surf. Sci. 171, 239 (1986).
15. B.M. Biwer, S.L. Bernasek, Surf. Sci. 167, 207 (1986).
16. Ph. Staib, H.F. Dylla, S.M. Rossnagel, J. Vac. Sci. Technol. 17, 291 (1980).
17. L.A. Casper, C.J. Powell (Eds.), "Industrial Applications of Surface Analysis", ACS Symp. Ser. 199, Chap. 16, Washington, D.C. (1982).
18. Y. Hirohata, S. Adachi, S. Fukuda, M. Mohri, T. Yamashina, N. Noda, S. Tanahashi, J. Fujita, Y. Gomay, J. Nucl. Mat. 122/123, 1160 (1984).
19. H. Moers, KfK-Report 4073 (1986).
20. R. Kaufmann, Master thesis, University of Karlsruhe (1984).
21. J.A. Shirley, Phys. Rev. B5, 4709 (1972).
22. H.J. Mathieu, J.B. Mathieu, D.G. McClure, D. Landolt, J.Vac. Sci. Technol. 14, 1023 (1977).
23. G.D. Davis, M. Natan, K.A. Anderson, Appl. Surf. Sci. 15, 321 (1983).
24. O. Kubaschewski, Atomic Energy Review Spec. Issue 9, 75 (1983).
25. G. Pfennig, H. Moers, H. Klewe-Nebenius, R. Kaufmann, H.J. Ache, Microchim. Acta, Supl. 11, 113 (1985).
26. K.S. Robinson, P.M.A. Sherwood, Surf. Interface Anal. 6, 261 (1984).

27. C.D. Wagner, L.H. Gale, R.H. Raymond, Anal. Chem. 51, 466 (1979).
28. D. Briggs, M.P. Seah (Eds.) "Practical Surface Analysis by Auger and X-ray Photoelectron Spectroscopy", Chapt. 3.4.3, J. Wiley, Chichester (1983).
29. O. Briggs, M.P. Seah (Eds.) "Practical Surface Analysis by Auger and X-ray Photoelectron Spectroscopy", Chapt. 3.3.1, J. Wiley, Chichester (1983).
30. K. Berresheim, private communication.
31. T.A. Carlson, "Photoelectron and Auger Spectroscopy", Plenum Press, New York (1975).
32. K.S. Kim, N. Winograd, Chem. Phys. Letters 31, 312 (1975).
33. J.H. Scofield, J. El. Spectrosc. Relat. Phenom. 8, 129 (1976).
34. K. Hauffe, "Oxidation of Metals", Plenum Press (1965).
35. E. Willin, M. Sirch, R.-D. Penzhorn, M. Devillers, to appear in Fusion Technology.